

High-dimensional modeling of spatial and spatio-temporal conditional extremes using INLA and the SPDE approach

E. S. Simpson^{*1}, T. Opitz², J. L. Wadsworth³

¹Department of Statistical Science, University College London, Gower Street, London, WC1E 6BT, U.K.

²Biostatistics and Spatial Processes, INRAE, Avignon, France.

³Department of Mathematics and Statistics, Lancaster University, LA1 4YF, U.K.

December 22, 2024

Abstract

The conditional extremes framework allows for event-based stochastic modeling of dependent extremes, and has recently been extended to spatial and spatio-temporal settings. After standardizing the marginal distributions and applying an appropriate linear normalization, certain non-stationary Gaussian processes can be used as asymptotically-motivated models for the process conditioned on threshold exceedances at a fixed reference location and time. In this work, we adopt a Bayesian perspective by implementing estimation through the integrated nested Laplace approximation (INLA), allowing for novel and flexible semi-parametric specifications of the Gaussian mean function. By using Gauss-Markov approximations of the Matérn covariance function (known as the Stochastic Partial Differential Equation approach) at a latent stage of the model, likelihood-based inference becomes feasible even with thousands of observed locations. We explain how constraints on the spatial and spatio-temporal Gaussian processes, arising from the conditioning mechanism, can be implemented through the latent variable approach without losing the computationally convenient Markov property. We discuss tools for the comparison of models via their posterior distributions, and illustrate the flexibility of the approach with gridded Red Sea surface temperature data at over 6,000 observed locations. Posterior sampling is exploited to study the probability distribution of cluster functionals of spatial and spatio-temporal extreme episodes.

Keywords: extremal dependence; conditional extremes model; latent Gaussian model; spatial extremes; threshold exceedances.

Acknowledgements

This publication is based upon work supported by the King Abdullah University of Science and Technology (KAUST) Office of Sponsored Research (OSR) under Award No. OSR-2017-CRG6-3434.02. The sea surface temperature data studied in this paper were provided by GHRSSST, Met Office and CMEMS.

^{*}Corresponding author. Email address: emma.simpson@ucl.ac.uk

1 Introduction

1.1 Statistical modeling of spatial extremes

The availability of increasingly detailed spatial and spatio-temporal datasets has motivated a recent surge in methodological developments to model such data. In this work, we are concerned with modeling extreme values of spatial or spatio-temporal processes, which we denote by $\{Y(s) : s \in \mathcal{S} \subseteq \mathbb{R}^2\}$ and $\{Y(s, t) : (s, t) \in \mathcal{S} \times \mathcal{T} \subseteq \mathbb{R}^2 \times \mathbb{R}_+\}$. The goal of modeling spatio-temporal extremes is often to enable extrapolation from observed extreme values to future, more intense episodes, and consequently requires careful selection of models suited to this delicate task.

Early work on spatial extremes focused almost exclusively on max-stable processes (Smith, 1990; Coles, 1993; Schlather, 2002; Padoan et al., 2010; Davison and Gholamrezaee, 2012). These are the limiting objects that arise through the operation of taking pointwise maxima of n weakly dependent and identically distributed copies of a spatial process. However, this is a poor strategy when data exhibit a property known as *asymptotic independence*, which means that the limiting process of maxima consists of everywhere-independent random variables. Moreover, even when the process is *asymptotically dependent*, meaning that the limit has spatial coherence, the fact that the resulting process is formed from many underlying original events (Dombry and Kabluchko, 2018) can hinder both interpretability and inference. More recently, analogues of max-stable processes suited to event-level data have been developed (Ferreira and de Haan, 2014; Dombry and Ribatet, 2015; Thibaud and Opitz, 2015; de Fondeville and Davison, 2021), but use of these generalized Pareto or r -Pareto processes also requires strong assumptions on the extremal dependence structure.

Broadly, spatial process data can be split according to whether they exhibit asymptotic independence or asymptotic dependence. As mentioned, these can be characterized by whether the data display independence or dependence in the limiting distribution of pointwise maxima, but when considering threshold exceedances other definitions are more useful. Consider two spatial locations $s, s+h \in \mathcal{S}$. For $Y(s) \sim F_s$, define the tail correlation function (Strokorb et al., 2015) as

$$\chi(s, s+h) = \lim_{q \rightarrow 1} \Pr\{F_{s+h}(Y(s+h)) > q | F_s(Y(s)) > q\}. \quad (1)$$

If $\chi(s, s+h) = 0$ for all $h \neq 0$ then Y is asymptotically independent, or asymptotically dependent where limit (1) is positive for all h . Intermediate scenarios of asymptotic dependence up to a certain distance are also possible. Asymptotic dependence is a minimum requirement for use of max-stable or Pareto process models, but in practice more rigid assumptions are imposed as these models do not allow for any weakening of dependence with the level of the event — a feature common in most environmental datasets.

Recent work on modeling of spatial extremes has focused on the twin challenges of incorporating flexible extremal dependence structures, and developing models and inference techniques that allow for large numbers of observation locations. Huser et al. (2017, 2021) suggest Gaussian scale mixture models, for which both types of extremal dependence can be captured depending on the distribution of the scaling variable. The model of Huser and Wadsworth (2019) was the first to offer a smooth transition between dependence classes, meaning it is not necessary to make a choice before fitting the model. However, owing to complicated likelihoods, each of these models is limited in practice to datasets with tens of observation locations. Modifications in Zhang et al. (2021) suggest that hundreds of sites might be possible, but further scalability looks elusive for now.

Wadsworth and Tawn (2019) proposed an alternative approach based on a spatial adaptation of the multivariate conditional extreme value model (Heffernan and Tawn, 2004; Heffernan and Resnick, 2007), which has been further extended to the space-time case by Simpson and Wadsworth (2021). Both types of extremal dependence can be handled and the likelihoods involved are much simpler. However, application thus far has still been limited

to hundreds of observation locations. In this work, we seek to exploit the power of Gaussian Markov random fields and the integrated nested Laplace approximation (INLA) in this context in order to permit truly high-dimensional inference and prediction, and to achieve more flexible modeling by replacing parametric structures with semi-parametric extensions. We note that, in the restricted case of Pareto processes, [de Fondeville and Davison \(2018\)](#) perform inference for a 3600-dimensional problem via a gradient-score algorithm. In this work, we handle inference for problems of comparable dimension, using the more flexible conditional extremes models with likelihood-based inference. [Opitz et al. \(2018\)](#) have previously used INLA in an extreme value analysis context, focusing on regression modeling of threshold exceedances, but this is the first time it has been utilized in the conditional extremes framework.

Throughout the remainder of the introduction, we provide background on conditional extremes models, and set up how we will modify the modeling assumption to enable inference through a latent variable approach, which allows inference to be performed using INLA. Use of these tools, combined with sparse approximations to the latent Gaussian field, is what permits inference to become feasible at thousands of observation locations.

1.2 Conditional extremes models

The aforementioned conditional extremes approaches, originating with [Heffernan and Tawn \(2004\)](#) in the multivariate case, involve the construction of models by conditioning on exceedances of a high threshold in a single variable. The spatial setting studied by [Wadsworth and Tawn \(2019\)](#), and subsequent spatio-temporal extension of [Simpson and Wadsworth \(2021\)](#), require conditioning on threshold exceedances at a single spatial or spatio-temporal location, with additional structure being introduced by exploiting the proximity of the other locations to this conditioning site.

In the spatial setting, denote by $\{X(s) : s \in \mathcal{S}\}$ a stationary and isotropic process with marginal distributions possessing exponential upper tails, i.e., $\Pr\{X(s) > x\} \sim e^{-x}$ as $x \rightarrow \infty$. This is achieved in practice via a marginal transformation, explained further in [Section 3.2](#). Let s_0 denote the conditioning site. We assume that $\{X(s)\}$ possesses a joint density, so that conditioning on the events $\{X(s_0) > u\}$ or $\{X(s_0) = u\}$ as $u \rightarrow \infty$ leads to the same limiting process ([Wadsworth and Tawn, 2019](#)); see also [Drees and Janßen \(2017\)](#) for further discussion on the conditioning event in a multivariate setting. We comment on handling anisotropy in [Section 6](#).

For a finite set of locations s_1, \dots, s_d , [Wadsworth and Tawn \(2019\)](#) assume that there exist normalizing functions $a_{s-s_0}(\cdot)$ and $b_{s-s_0}(\cdot)$ such that as $u \rightarrow \infty$,

$$\Pr \left(\left[\frac{X(s_i) - a_{s_i-s_0} \{X(s_0)\}}{b_{s_i-s_0} \{X(s_0)\}} \right]_{i=1, \dots, d} \leq \mathbf{z} \mid X(s_0) = u \right) \rightarrow \Pr(\{Z^0(s_i)\}_{i=1, \dots, d} \leq \mathbf{z}), \quad (2)$$

where $\mathbf{z} = (z_1, \dots, z_d)$. Several theoretical examples are provided therein to illustrate this assumption. The process $\{Z^0(s)\}$ is referred to as the residual process. The first of the normalizing functions is constrained to take values $a_0(x) = x$ and $a_{s-s_0}(x) \in [0, x]$, and is usually non-increasing as the distance between s and s_0 increases: the residual process therefore satisfies $Z^0(s_0) = 0$. Furthermore, under assumption (2), the excess of the conditioning variable $X(s_0) - u \mid X(s_0) > u$ is exponentially distributed, and independent of the residual process.

Assumption (2) is exploited for modeling by assuming that it holds approximately above a high threshold u . In particular, we assume

$$\{X(s) : s \in \mathcal{S}\} \mid [X(s_0) = x] = a_{s-s_0}(x) + b_{s-s_0}(x)\{Z^0(s) : s \in \mathcal{S}\}, \quad x > u. \quad (3)$$

We note that assumptions (2) and (3) depend on the choice of s_0 . In some applications, there may be a location of particular interest that would make a natural candidate for s_0 , but for other scenarios the choice is not evident.

However, under the assumption that $\{X(s)\}$ possesses a stationary dependence structure, in the sense that the joint distributions are invariant to translation, the form of the normalization functions a_{s-s_0} , b_{s-s_0} and the residual process $\{Z^0(s)\}$ do not in fact depend on s_0 , so that inference made using one conditioning location is applicable at any location. We discuss this issue further in Section 3.8.

Suitable choices for a_{s-s_0} , b_{s-s_0} and $\{Z^0(s)\}$ lead to models with different features. Wadsworth and Tawn (2019) propose a theoretically-motivated parametric form for the normalizing function $a_{s-s_0}(\cdot)$, as well as three different parametric models for $b_{s-s_0}(\cdot)$ that are able to capture different tail dependence features. They propose constructing the residual process by first considering some stationary Gaussian process $\{Z(s)\}$, and either subtracting $Z(s_0)$ or conditioning on $Z(s_0) = 0$ to ensure the condition $Z^0(s_0) = 0$ on $\{Z^0(s)\}$ is satisfied. Marginal transformations of $\{Z^0(s)\}$ are considered therein in order to increase the flexibility of models, but here we keep the Gaussian margins to facilitate computation. Their approach to inference involves a composite likelihood to allow different locations to play the role of the conditioning site, and combine information across each of these.

Inference under this “vanilla” version of the model can be performed for hundreds of observation locations. However, scalability to thousands of locations is impeded by the $O(d^3)$ -complexity of matrix inversion in the Gaussian process part of the likelihood, and the fact that, in contrast to other areas of spatial statistics, we have n replicates of the process to be used for inference. By using a latent variable approach, where the dimension of the latent process can be chosen independently of the number of spatial locations to be modeled, the number of observation locations could be increased substantially.

To carry out inference for conditional extremes models in this latent variable setting, we propose using the INLA framework, with a latent Gaussian process characterized by a Markovian structure, such that precision matrices (i.e., inverse covariance matrices) are sparse. A benefit of this Bayesian approach to statistical modeling with latent variables, over alternatives like the EM algorithm or Laplace approximations applied in a frequentist setting, is that parameters, predictions and uncertainties can be estimated simultaneously, and prior distributions can be used to incorporate expert knowledge and control the complexity of the model or its components with respect to simpler baselines. Moreover, the availability of the R software package R-INLA (Rue et al., 2017) facilitates the implementation, reusability and adaptation of our models and code, making them suitable for use with datasets other than the one considered in this paper. One of the main challenges we face is reconciling the form of the conditional extremes models with formulations allowed under this framework. We outline our general strategy in the following section, but defer more detailed computational and implementation details to Section 5. Our motivation for this is to provide readers with a general understanding of the methodology, unimpeded by extensive technical details. However, we note that implementation is a substantial part of the task and therefore Section 5 provides interested parties with the necessary particulars.

1.3 Modification to incorporate the latent variable approach

Under the latent variable framework, described in detail in Section 2.1, we make the minor modification of modeling assumption (3) to

$$X(s_i)|[X(s_0) = x] = a_{s_i-s_0}(x) + b_{s_i-s_0}(x)Z^0(s_i) + \epsilon_i, \quad \epsilon_i \sim \mathcal{N}(0, \sigma^2) \text{ i.i.d.}, \quad (4)$$

for $i = 1, \dots, d$, and assume $\epsilon_0 = 0$ at s_0 . Suppose that we write $\tilde{X}^0(s_i) = a_{s_i-s_0}(x) + b_{s_i-s_0}(x)Z^0(s_i)$, $i = 1, \dots, d$. The appearance of the i.i.d. Gaussian noise component allows the effective dimensionality of the latent variables $(\tilde{X}^0(s_1), \dots, \tilde{X}^0(s_d))$ to be less than d . This means that we do not need to directly manipulate the d -variate distribution of $Z^0(s_i)$ for the $i = 1, \dots, d$ sites. Instead, it suffices to manipulate the m -variate distribution of $\{Z^0(s)\}$ using a much smaller collection of $m \ll d$ locations, that is, to define a “low-rank” representation of $\{Z^0(s)\}$

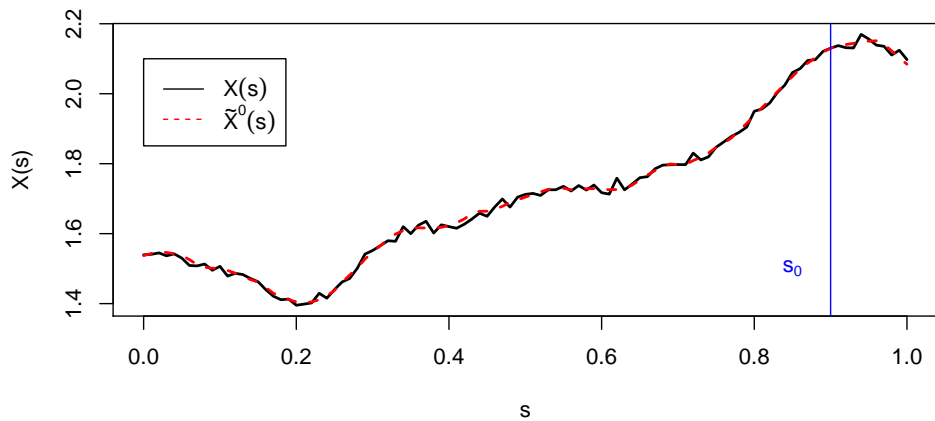


Figure 1: Illustration of process $\{X(s)\}$ and $\{\tilde{X}^0(s)\}$.

and to use linear spatial interpolation to approximate the values elsewhere. Consequently, the noise component represents a convenient device for efficient inference, and in most cases where data realizations are smooth we would anticipate estimates of its variance σ^2 to be very small. In particular, the Gaussian noise is not representing a so-called “nugget effect” in order to capture measurement error or add extra roughness to the process. The processes $\{X(s)\}$ and $\{\tilde{X}^0(s)\}$, which depends on the choice of s_0 , are illustrated in Figure 1.

In addition to the gains made by only needing to evaluate the covariance matrix of an m -dimensional vector, the use of Gauss-Markov approximations to the random field ensures that precision matrices are sparse, which also speeds up computation time.

1.4 Overview of paper

The remainder of the paper is structured as follows. In Section 2, we provide flexible forms for the conditional spatial extremes model that are possible under the latent variable framework. We apply our inferential approach for modeling conditional spatial extremes to a dataset of Red Sea surface temperatures in Section 3, and consider a range of diagnostics to aid model selection and the assessment of model fit. A spatio-temporal extension is presented in Section 4. Section 5 is aimed at those readers interested in the specifics of implementation, and includes more detail on the stochastic partial differential equation (SPDE) approach used to generate numerically convenient approximations to the Matérn covariance and implementation in R-INLA. Section 6 concludes with a discussion. Supplementary Material contains code for implementing the models we develop, and is available at <https://github.com/essimpson/INLA-conditional-extremes>.

2 Model formulations

In this section, we discuss specific variants of model (4), focusing on forms of the normalizing functions that are possible using the INLA methodology. We begin by outlining details of the latent variable approach.

2.1 Generalities on the latent variable approach

Here, we provide some general details on the latent variable approach for spatial modeling, denoting the observed data generically by $\mathbf{V} = (V_1, \dots, V_d)^\top$, which in our context will correspond to observations at d spatial locations. When modeling spatial extreme values, it is always necessary to have replications of the spatial process in question in order to distinguish between marginal distributions and dependence structures, and to define extreme events. We comment further on the handling of temporal replication in Sections 5.5 and 5.6; we will later also explicitly model temporal, as well as spatial, dependence.

In hierarchical modeling with latent Gaussian processes, we define a latent, unobserved Gaussian process $\mathbf{W} = (W_1, \dots, W_m)^\top$, with m denoting the number of spatial locations of the latent process in our setting, and we assume conditional independence of the observations \mathbf{V} with respect to \mathbf{W} . We use the so-called *observation matrix* $A \in \mathbb{R}^{d \times m}$ to define a linear predictor

$$\boldsymbol{\eta} = \boldsymbol{\eta}(\mathbf{W}) = A\mathbf{W}$$

that linearly combines the latent variables in \mathbf{W} into components η_i associated with V_i , $i = 1, \dots, d$. The components η_i represent a parameter of the probability distribution of V_i . The matrix A is deterministic and is fixed before estimating the model. For instance, A handles the spatial interpolation from the m locations of the latent Gaussian field $\{Z(s)\}$ towards the d observed sites as outlined in Section 1.3; for this, \mathbf{W} may contain the values of a spatial field at locations $\tilde{s}_1, \dots, \tilde{s}_m$, and A has i -th line $A_i = (0, \dots, 0, 1, 0, \dots, 0)$ if the observation location s_i of V_i coincides with one of the locations \tilde{s}_{j_0} , where the 1-entry is at the j_0 th position. Otherwise, several entries of A_i could have non-zero weight to implement interpolation between the \tilde{s}_j -locations. The distribution of $\boldsymbol{\eta}$ is also multivariate Gaussian due to the linear transformation. The univariate probability distribution of V_i , often referred to as the *likelihood model*, can be Gaussian or non-Gaussian and is parametrized by the linear predictor η_i , and potentially by other hyperparameters related to the shape of the distribution. The vector of hyperparameters (i.e., of parameters that are not components of one of the Gaussian vectors \mathbf{W} and $\boldsymbol{\eta}$), such as those related to variance, spatial dependence range, or smoothness of a spline curve, is denoted by $\boldsymbol{\theta}$. Letting $\pi(\cdot)$ denote a generic probability distribution, the hierarchical model is structured as follows:

$$\begin{aligned} \boldsymbol{\theta} &\sim \pi(\cdot) && \text{hyperparameters,} \\ \mathbf{W} \mid \boldsymbol{\theta} &\sim \mathcal{N}_m(\mathbf{0}, Q(\boldsymbol{\theta})^{-1}) && \text{latent Gaussian components,} \\ V_i \mid \mathbf{W}, \boldsymbol{\theta} &\sim \pi(\cdot \mid \eta_i, \boldsymbol{\theta}), \text{ independent} && \text{likelihood of observations.} \end{aligned}$$

The matrix $Q(\boldsymbol{\theta})$ denotes the precision matrix of the latent Gaussian vector \mathbf{W} , whose variance-covariance structure may depend on some of the hyperparameters in $\boldsymbol{\theta}$ that we seek to estimate. In the case of observations V_i having a Gaussian distribution, the conditional variance σ^2 of V_i given η_i is a hyperparameter, and we define

$$V_i \mid \eta_i, \sigma^2 \sim \mathcal{N}(\eta_i, \sigma^2), \quad i = 1, \dots, d.$$

If $d > m$ as in our setting, we need a small positive variance $\sigma^2 > 0$ since there is no observation matrix A that would allow for an exact solution to the equation $\mathbf{V} = A\mathbf{W}$ with given \mathbf{V} . If the data-generating process is smooth then $\sigma^2 > 0$ could be fixed to a very small value, but for reasons of stabilizing the estimation procedure, it may be preferable to estimate its value from the data. This is the approach we take.

A major benefit of the construction with latent variables is that the dimension of the latent vector \mathbf{W} is not directly determined by the number of observations d . The computational complexity and stability of matrix operations (e.g., determinants, matrix products, solution of linear systems) arising in the likelihood calculations for the above Bayesian hierarchical model is therefore mainly determined by the tractability of the precision matrix

$Q(\boldsymbol{\theta})$, whose dimension can be controlled independently from the number of observations. Such matrix operations can be implemented very efficiently if precision matrices are sparse (Rue and Held, 2005). If data are replicated many times with dependence between replications, such as spatial data observed at regular time steps in spatio-temporal modeling, the sparsity property can be preserved in the precision matrix of the latent space-time process \mathbf{W} . Here, we will make assumptions related to the separability of space and time, which allows us to generate sparse space-time precision matrices by combining sparse precision matrices of a purely spatial and a purely temporal process; see Sections 5.5 and 5.6 for further details.

2.2 Proposed models

As mentioned in Section 1.2, Wadsworth and Tawn (2019) propose parametric forms of the normalizing functions $a_{s-s_0}(x)$ and $b_{s-s_0}(x)$. To enforce asymptotic dependence, we simply take $a_{s-s_0}(x) = x$ and $b_{s-s_0}(x) = 1$, but allowing the form of these functions to depend on the distance from the conditioning location is the key aspect that enables modeling of asymptotic independence as well. Under the INLA framework, it is possible to impose parametric forms on $a_{s-s_0}(x)$, such as the one proposed by Wadsworth and Tawn (2019) where parameters do not contribute linearly to the predictor $\boldsymbol{\eta}$. In this case, the parameters of $a_{s-s_0}(x)$ are part of the hyperparameter vector $\boldsymbol{\theta}$, whose dimension must remain moderate (at most 10 to 20 components), since INLA must perform numerical integration with integrand functions defined on the hyperparameter space. Alternatively, semi-parametric forms can be implemented by considering the function $a_{s-s_0}(x)$ as a component of the linear predictor $\boldsymbol{\eta}$. This provides the benefit of increased flexibility, and is computationally convenient since INLA can handle a large number of latent Gaussian variables in \mathbf{W} when calculating accurate deterministic approximations to posterior distributions, thanks to Laplace approximation techniques. We focus on the semi-parametric solution for its novelty and computational convenience. The second normalizing function, $b_{s-s_0}(x)$, must have a parametric form with a small number of parameters included in the hyperparameter vector $\boldsymbol{\theta}$, because it is not possible to represent both $b_{s-s_0}(x)$ and $\{Z^0(s)\}$ as latent Gaussian components, given the restriction of using a linear transformation from \mathbf{W} to $\boldsymbol{\eta}$. We next discuss the options in detail.

For the first normalizing function, pertaining to the mean of the Gaussian process of conditional extremes, we set $a_{s-s_0}(x) = x \cdot \alpha(s-s_0)$, and propose the use of a spline function for $\alpha(s-s_0)$, i.e., a semi-parametric model. This function is constrained to have $\alpha(0) = 1$, ensuring that $a_0(x) = x$. In extension to the models for conditional spatial and spatio-temporal extremes developed by Wadsworth and Tawn (2019) and Simpson and Wadsworth (2021), we can further increase the flexibility of the conditional mean model by explicitly including a second spline function, denoted $\gamma(s-s_0)$ and with $\gamma(0) = 0$, that is not multiplied by the value of the process at the conditioning site. An example where such a deterministic component arises is given by the conditional extremes model corresponding to the Brown–Resnick type max-stable processes (Kablichko et al., 2009) with log-Gaussian spectral function (see Proposition 4 of Dombry et al., 2016), which are widely used in statistical approaches based on the asymptotically dependent limit models mentioned in Section 1. In this case, we obtain

$$X(s) \mid [X(s_0) = x] \stackrel{d}{=} x + Z(s) - Z(s_0) - \text{Var}(Z(s) - Z(s_0))/2,$$

with a centered Gaussian process $\{Z(s)\}$. Therefore, by setting $a_{s-s_0}(x) = x$, in this model the γ -term corresponds to the semi-variogram $\text{Var}(Z(s) - Z(s_0))/2$. We note that for the Brown–Resnick process, γ should indeed correspond to a valid semi-variogram, although we will not constrain it as such in our implementation.

For the second normalizing function, which influences the variance of the Gaussian process of conditional extremes, we consider one of the forms proposed by Wadsworth and Tawn (2019), setting $b_{s-s_0}(x) = x^\beta$, $\beta \in [0, 1)$. In the framework set by the implementation of INLA in R-INLA, estimation of the parameter β requires the use of

generic models, which we describe in Section 5.6. An alternative to this is to carry out inference for a range of β values and select an appropriate one using model selection tools, such as those that will be discussed in Section 3.5, but we prefer estimation of β over this approach. A special case of this model involves setting $\beta = 0$, yielding $b_{s-s_0}(x) = 1$; this offers a simpler model which may be sufficient in some cases. We emphasize that the use of generic R-INLA models allows for the implementation of other relevant parametric forms for the function b_{s-s_0} , if the above choice does not provide a satisfactory fit. In our implementation, we place a log-Gaussian prior on β , as will be discussed in Section 3.4. This does not guarantee estimates of $\beta < 1$, but such a constraint could be included within the generic-model framework if required.

In the implementation of the conditional spatial extremes assumption using R-INLA, we therefore propose to explore several options for the form of the model: setting $\alpha(s-s_0) = 1$ everywhere or using a spline function; whether or not to include the second spline term $\gamma(s-s_0)$; and whether or not to include the parameter β . Together, this means that all models can be written as special cases of the representation

$$X(s_i)|[X(s_0) = x] = \alpha(s_i - s_0)x + \gamma(s_i - s_0) + x^\beta Z^0(s_i) + \epsilon_i, \quad x > u, \quad i = 1, \dots, d, \quad (5)$$

where we suppose that $\{Z^0(s)\}$ has a Gaussian structure, further described in Sections 5.3 and 5.4, and $\epsilon_i \sim \mathcal{N}(0, \sigma^2)$ i.i.d.. This opens up the framework of conditional Gaussian models and the potential for efficient inference via INLA, while closely following the conditional extremes formulation. In particular, the joint distribution of $\{X(s_i) : i = 1, \dots, d\}$, not conditional on the value of $X(s_0)$, is non-Gaussian.

We now give an illustration, linking model (5) to the general notation and principles outlined in Section 2.1. Our observation vector \mathbf{V} is the process $\{X(s)\}$ observed at d locations: $\mathbf{X} = (X(s_1), \dots, X(s_d))^\top$. The latent Gaussian component \mathbf{W} consists of components for α, γ and $\{Z^0(s)\}$: $\mathbf{W} = (\mathbf{W}_\alpha^\top, \mathbf{W}_\gamma^\top, \tilde{\mathbf{Z}}^{0\top})^\top \in \mathbb{R}^{m_\alpha} \times \mathbb{R}^{m_\gamma} \times \mathbb{R}^{m_z}$, with $m_\alpha + m_\gamma + m_z = m$. The observation matrix $A \in \mathbb{R}^{d \times m}$ is the concatenation of matrices for each component: $A_\alpha \in \mathbb{R}^{d \times m_\alpha}$, $A_\gamma \in \mathbb{R}^{d \times m_\gamma}$, and $A_S \in \mathbb{R}^{d \times m_z}$. We include the x^β -term into the process $\tilde{\mathbf{Z}}^0$ if we want to estimate the parameter β , such that it does not appear in the fixed observation matrix A_S ; if β is fixed, we could instead include the x^β -term into A_S . All together, we get

$$\mathbf{X}|[X(s_0) = x] = (A_\alpha, A_\gamma, A_S)(\mathbf{W}_\alpha^\top, \mathbf{W}_\gamma^\top, \tilde{\mathbf{Z}}^{0\top})^\top + \boldsymbol{\epsilon},$$

with i.i.d. Gaussian components in $\boldsymbol{\epsilon} = (\epsilon_1, \dots, \epsilon_d)^\top$.

To implement model (5) in an efficient manner for a large number of observation locations, we need to carefully consider computations related to the residual process $\{Z^0(s)\}$. This is explained in detail in Section 5.4. In Section 3, we apply variants of the model to the Red Sea surface temperature data, with the different model forms summarized in Table 1.

3 Inference for conditional spatial extremes

3.1 Overview

In this section, we propose specific model structures for the general model (5) and illustrate an application of our approach using a dataset of Red Sea surface temperatures, the spatio-temporal extremes of which have also been studied by Hazra and Huser (2021) and Simpson and Wadsworth (2021), for instance. We focus on the purely spatial case here, and consider further spatio-temporal modeling extensions for this dataset in Section 4. We begin with an introduction to the data, and a discussion of the transformation to exponential-tailed marginal distributions required for conditional extremes modeling. We then consider variants of the conditional spatial model, based on the possibilities introduced in Section 1.3, and use a range of diagnostics to assess their relative suitability for

modeling the Red Sea data. For the best-fitting model, we present additional results, and conclude with a discussion of consequences of using a single, fixed conditioning site. Throughout this section, the threshold u in conditional model (5) is taken to be the 0.95 quantile of the transformed data, following [Simpson and Wadsworth \(2021\)](#). For the sake of a brevity, we do not compare results for different thresholds in the following.

3.2 Red Sea surface temperature data

The surface temperature dataset comprises daily observations for the years 1985 to 2015 for 16703 locations across the Red Sea, corresponding to $0.05^\circ \times 0.05^\circ$ grid cells. We focus only on the months of July to September to approximately eliminate the effects of seasonality. More information on the data, which were obtained from a combination of satellite and in situ observations, can be found in [Donlon et al. \(2012\)](#). Extreme events in this dataset are of interest, since particularly high water temperatures can be detrimental to marine life, e.g., causing coral bleaching, and in some cases coral mortality.

[Simpson and Wadsworth \(2021\)](#) apply their conditional spatio-temporal extremes model to a subset of 54 grid cells located across the north of the Red Sea. In this paper, we instead focus on a southern portion of the Red Sea, where coral bleaching is currently more of a concern ([Fine et al., 2019](#)). We demonstrate our approach using datasets of two different spatial dimensions; the first dataset contains 6239 grid cells, corresponding to all available locations in our region of interest, while the second dataset is obtained by taking locations at every third longitude and latitude value in this region, leaving 678 grid cells to consider. These two sets of spatial locations are shown in [Figure 2](#). [Simpson and Wadsworth \(2021\)](#) consider their 54 spatial locations at five time-points, resulting in a lower dimensional problem than both the datasets we consider here. On the other hand, [Hazra and Huser \(2021\)](#) model the full set of 16703 grid cells, but they ensure computational feasibility by implementing so-called ‘low-rank’ modeling techniques using spatial basis functions given by the dominant empirical orthogonal functions, obtained from preliminary empirical estimation of the covariance matrix of the data.

As our study region lies away from the equator, one degree in latitude and one degree in longitude correspond to different distances. To correct for this we apply a transformation, multiplying the longitude and latitude values by 1.04 and 1.11, respectively, such that spatial coordinates are expressed in units of approximately 100 km. We use the Euclidean distance on these transformed coordinates to measure spatial distances in the remainder of the paper.

To ensure the marginal distributions of the data have the required exponential upper tails, we transform to Laplace scale, as proposed by [Keef et al. \(2013\)](#). This is achieved using a semiparametric transformation. Let Y denote the surface temperature observations at a single location. We assume these observations follow a generalized Pareto distribution above some high threshold v , and use an empirical distribution function below v , denoted $\tilde{F}(\cdot)$. That is, we assume the distribution function

$$F(y) = \begin{cases} 1 - \lambda_v \left\{ 1 + \frac{\xi(y-v)}{\sigma_v} \right\}_+^{-1/\xi}, & y \geq v \\ \tilde{F}(y), & y < v, \end{cases}$$

for $\lambda_v = 1 - F(v)$, $\sigma_v > 0$ and $y_+ = \max(y, 0)$. In practice, we take v to be the empirical 0.95 quantile of Y , so that $\lambda_v = 0.05$. Having fitted this model, we obtain standard Laplace margins via the transformation

$$X = \begin{cases} \log \{2F(Y)\}, & F(Y) \leq 1/2, \\ -\log [2\{1 - F(Y)\}], & F(Y) > 1/2. \end{cases}$$

This transformation is applied separately for each spatial location, with the parameters of the generalized Pareto distributions estimated using the `ismev` package in R ([Heffernan and Stephenson, 2018](#)). It is possible to include

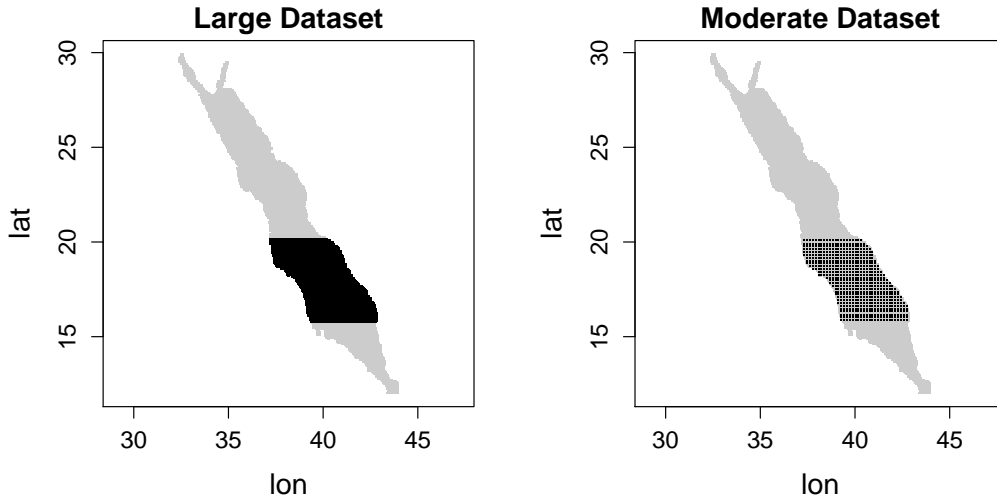


Figure 2: Location of the Red Sea (grey), and the subsets of grid cells in the two datasets we consider (black).

covariate information in the marginal parameters and impose spatial smoothness on these, for instance by using flexible generalized additive models (see [Castro-Camilo et al. \(2021\)](#) for details), but we do not take this approach.

3.3 Variants of the spatial model

In Section 2.2, we discussed choices of the normalizing functions $a_{s-s_0}(x)$ and $b_{s-s_0}(x)$ that are possible under the INLA framework. In Table 1, we summarize the models we consider based on the alternative normalizing functions. We will compare these models for the Red Sea data using the Watanabe-Akaike information criterion (WAIC) and conditional predictive ordinate (CPO), discussed in Sections 3.5 and 3.6, respectively. In Section 3.6, we consider a further cross validation procedure, summarized by the root mean square error (RMSE), also presented in Table 1. In addition, the computation times for each model are included in Table 1, as this information may also aid model selection where there is similar performance under the other criteria.

Model 0 has $a_{s-s_0}(x) = x$, $b_{s-s_0}(x) = 1$, resulting in a very simple asymptotically dependent model. Model 2 is also asymptotically dependent, but allows for weaker dependence than in Model 0 due to the drift that is captured by the $\gamma(s - s_0)$ term, supposed to be negative in practice based on the remarks following equation (5). In Model 6, the residual process has been removed, so that all variability is forced to be captured by the nugget process ϵ_i in (5). Models 0 and 6 are meant to act as simple baselines to which we can compare the other models, but we would not expect them to perform sufficiently well in practice. As will be detailed in Section 5.4, we focus on a residual process of the form $\{Z(s)\} - Z(s_0)$ for all of these models.

In the remainder of this section, we apply these models to the Red Sea data with the large spatial dataset in Figure 2, and discuss model selection and diagnostic techniques. For the conditioning site, we selected a location lying towards the centre of the spatial domain of interest. We discuss this choice further in Section 3.8, where we present additional results based on the moderate dataset. In Appendix A, we provide an initial assessment of the spatial extremal dependence properties of the sea surface temperature data, based on the tail correlation function defined in (1). These results demonstrate that there is weakening dependence in the data at increasingly extreme levels, which indicates that models for asymptotic independence should be more appropriate here.

Model number	Model form	WAIC	CPO	RMSE	Run-time
0	$x + \{Z^0(s)\}$	2438	-0.0061	0.019	20
1	$x \cdot \alpha(s - s_0) + \{Z^0(s)\}$	614	-0.0028	0.001	22
2	$x + \gamma(s - s_0) + \{Z^0(s)\}$	743	-0.0035	0.005	35
3	$x \cdot \alpha(s - s_0) + \gamma(s - s_0) + \{Z^0(s)\}$	4	-0.0018	0	32
4	$x \cdot \alpha(s - s_0) + \gamma(s - s_0) + x^\beta \cdot \{Z^0(s)\}$	0	0	0.003	107
5	$x \cdot \alpha(s - s_0) + x^\beta \cdot \{Z^0(s)\}$	611	-0.0004	0.010	86
6	$x \cdot \alpha(s - s_0) + \gamma(s - s_0)$	4394961	-2.8042	0.514	43

Table 1: Summary of conditional spatial models, model selection criteria, and total run-times (minutes). The minimum WAIC value (-1460982 for Model 4); maximum CPO value (3.0305 for Model 4); and minimum RMSE value (0.862 for Model 3) have been subtracted from their respective columns. We estimate β as 0.29 with a 95% credible interval of (0.27, 0.31) (Model 4) and 0.33 (0.31, 0.34) (Model 5).

3.4 The mesh and choices of prior distributions for hyperparameters

We explain all the technical details of the construction of spatial and spatio-temporal precision matrices Q and observation matrices A in Section 5. Gauss–Markov distributions with approximate Matérn covariance are achieved through the SPDE approach of Lindgren et al. (2011). It requires the definition of a triangulation covering the study area. The locations of the components of the multivariate Gaussian vector defining the latent spatial process are located at the nodes of the triangulation. To generate this spatial discretization of the latent Gaussian process, and the observation matrix A to link it to observations, we use the mesh shown in Figure 3. The spatial triangulation mesh has 541 nodes, i.e., the dimension of the latent process is approximately 8.7% of the size of the large dataset, and similar in size to the moderate dataset. The mesh was generated using R-INLA, with the most dense region corresponding to the area where we have observations. The extension of the mesh beyond the study region is reasonably big, in order to avoid boundary effects of the SPDE for the sea surface temperatures, whose spatial dependence range is known to be relatively large; see Simpson and Wadsworth (2021). We use a coarser resolution in the extension region to keep the number of latent Gaussian variables as small as reasonably possible.

For specifying the prior distributions of the hyperparameters (e.g., variances, spatial ranges, autocorrelation coefficients) we use the concept of penalized complexity (PC) priors (Simpson et al., 2017), which has become the standard approach in the INLA framework. PC priors control model complexity by shrinking model components towards a simpler baseline model, using a constant rate penalty expressed through the Kullback-Leibler divergence of the more complex model with respect to the baseline. In practice, only the rate parameter has to be chosen by the modeler, and it can be determined indirectly—but in a unique and intuitive way—by setting a threshold value r and a probability $p \in (0, 1)$ such that $\Pr(\text{hyperparameter} > r) = p$, with $>$ replaced by $<$ in some cases, depending on the role of the parameter. For example, the standard baseline model for a variance parameter of a latent and centered Gaussian prior component \mathbf{W} contributing to the linear predictor $\boldsymbol{\eta}$ is a variance of 0, which corresponds to the absence of this component from the model, and the PC prior of the standard deviation corresponds to an exponential distribution. Analogously, we can fix the PC prior for the variance parameter σ^2 of the observation errors ϵ_i in (4). For the Matérn covariance function, PC priors are defined jointly for the range and the variance, with the baseline given by infinite range and variance 0; in particular, the inverse of the range parameter has a PC prior given by an exponential distribution, see Fuglstad et al. (2019) for details. For the temporal auto-correlation coefficient ρ , which is later defined in (8), the baseline could be either $\rho = 0$ (no dependence) or $\rho = 1$ (full dependence); here, we opt for $\rho = 0$. As explained by Simpson et al. (2017), PC priors are not useful to “regularize”

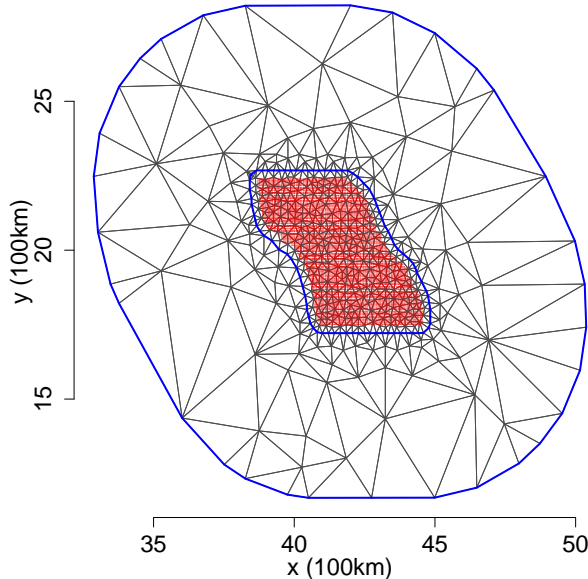


Figure 3: The large set of spatial locations (red dots) and the corresponding triangulation mesh used for the SPDE model with an inner and outer boundary (blue lines). The inner boundary delimits a high-resolution zone covering the study area, while the outer boundary delimits an extension zone with lower resolution to prevent effects of SPDE boundary conditions in the study area.

models, i.e., to select a moderate number of model components among a very large number of possible model components. Rather, they are used to control the complexity of a moderate number of well-chosen components that always remain present in the posterior model, and they do not put any positive prior mass on the baseline model.

Due to the availability of many observations in the Red Sea dataset, we found the hyperparameter priors to only have a small impact on posterior inference in our application, and that the credible intervals of the hyperparameters are very narrow. We have chosen moderately informative PC priors through the following specification:

$$\Pr(\rho > 0.5) = 0.5, \quad \Pr(\sigma > 0.1) = 0.5, \quad \Pr(\sigma_Z > 1) = 0.5, \quad \Pr(\rho_Z > 100 \text{ km}) = 0.5,$$

where σ_Z and ρ_Z are the standard deviation and the empirical range, respectively, of the unconstrained spatial Matérn fields $\{Z(s)\}$. For the β -parameter estimated in Models 4 and 5, we choose a log-normal prior where the normal has mean $-\log(2)$ and variance 1.

For the value of the SPDE parameter ζ , discussed in Section 5.3, we choose to fix $\zeta = 1.5$ for the spatial model ($D = 2$), corresponding to an exponential correlation. Sensitivity to ζ can be checked by comparing fitted models across different values, as demonstrated in Appendix B.2. We find this to have little effect on the results for our data.

For spline components with SPDE priors in $D = 1$, we have fixed the range to 100 km and the standard deviation to 0.5, since we consider that estimating these parameters is not crucial. This avoids very high computational cost arising when we estimate many hyperparameters with R-INLA. If we wished to obtain very smooth posterior estimates of the spline function, we could choose parameters that lead to stronger constraints on the (prior) variability of the spline curve. We use quadratic spline functions for both $\alpha(s - s_0)$ and $\gamma(s - s_0)$, which we found to provide more flexibility than their linear counterparts. The spline knots are chosen to be equidistant, with one knot at the boundary where $s = s_0$, and a further 14 interior knots. This quantity provides a reasonable balance between

the reduced flexibility that occurs when using too few knots, and the computational cost and numerical instability (owing to near singular precision matrices) that may arise with using too many. We will demonstrate the estimated spline functions for some of our models in Section 3.7.

3.5 Model selection using WAIC

Conveniently, implementation in R-INLA allows for automatic estimation of certain information criteria that can be used for model selection. Two such criteria are the deviance information criterion (DIC), and the widely applicable or Watanabe-Akaike information criterion (WAIC) of Watanabe (2013). We favour the latter since it captures posterior uncertainty more fully than the DIC. This, and other, benefits of the WAIC over the DIC are discussed by Vehtari et al. (2017), where an explanation of how to estimate the WAIC is also provided. Using our general notation for latent variable models, as in Section 2.1, suppose that the posterior distribution of the vector of model parameters $\tilde{\boldsymbol{\theta}} = (\boldsymbol{\theta}^\top, \mathbf{W}^\top)^\top$ is represented by a sample $\tilde{\boldsymbol{\theta}}^s$, $s = 1, \dots, S$, with the corresponding sample variance operator given by $\mathbb{V}_{s=1}^S(\cdot)$. Given the observations v_i , $i = 1, \dots, d$, the WAIC is then estimated as

$$\sum_{i=1}^d \log \left\{ \frac{1}{S} \sum_{s=1}^S \pi(v_i | \tilde{\boldsymbol{\theta}}^s) \right\} - \sum_{i=1}^d \mathbb{V}_{s=1}^S \left\{ \log \pi(v_i | \tilde{\boldsymbol{\theta}}^s) \right\},$$

with the first term providing an estimate of the log predictive density, and the second an estimate of the effective number of parameters. Within R-INLA, we do not generate a representative sample, but the sample means and variances with respect to $\tilde{\boldsymbol{\theta}}^s$ in the above equation are estimated based on R-INLA's internal representation of posterior distributions; see also the estimation technique for the DIC explained in Rue et al. (2009, Section 6.4).

We use the WAIC to compare each of the models in Table 1 applied to the large spatial dataset of Figure 2, with smaller WAIC values being preferred. Models 1 and 3 are simplified versions of Models 5 and 4, respectively, in that the value of β is fixed to 0 rather than estimated directly in R-INLA. In both cases, the results are very similar whether β is estimated or fixed, suggesting the simpler models are still effective.

The estimated WAIC values suggest Models 3 and 4 provide the best fit for our data. The common structure in these models are the terms $\alpha(s - s_0)x$ and $\gamma(s - s_0)$, indicating that their inclusion is important. In Model 4, the value of β is estimated to be 0.29, but despite simplifying the model, setting $\beta = 0$ as in Model 3 provides competitive results.

3.6 Cross validation

As mentioned previously, the main aim of fitting conditional extremes models is usually to extrapolate to extreme levels that have not been previously observed. However, the INLA framework also lends itself to the task of interpolation, e.g., making predictions for unobserved locations. Although interpolation is not our aim, here we discuss some procedures that allow for the assessment of models in this setting. For model selection, we can use cross-validated predictive measures, based on leave-one-out cross-validation (LOO-CV). These are relatively quick to estimate with INLA without the need to re-estimate the full model; see Rue et al. (2009, Section 6.3). Here, one possible summary measure is the *conditional predictive ordinate* (CPO), corresponding to the predictive density of observation v_i given all the other observations \mathbf{v}_{-i} , i.e.,

$$\text{CPO}_i = \pi(v_i | \mathbf{v}_{-i}),$$

for $i = 1, \dots, d$. Log-transformed values of CPO define the log-scores often used in the context of prediction and forecasting (Gneiting and Raftery, 2007). A model with higher CPO values usually indicates better predictions; we present the average value obtained for each model in Table 1. The results are relatively similar across Models

0 to 5, but clearly substantially better than Model 6, which we include purely for comparison. Model 6 performs poorly here since all spatially correlated residual variation has been removed. We note that the CPO is not usually used for extreme value models, and is not particularly informative here since the loss of information from holding out a single observation is negligible in the case of densely observed processes with very smooth surface. However, we include it as it may be useful for other applications where spatial and temporal interpolation are important, and due to the simplicity of its calculation in R-INLA.

One can also consider the *probability integral transform* (PIT) corresponding to the distribution function of the predictive density, evaluated at the observed value v_i , i.e.,

$$\text{PIT}_i = \int_{-\infty}^{v_i} \pi(v | \mathbf{v}_{-i}) dv.$$

If the predictive model for single hold-out observations appropriately captures the variability in the observed data, then the PIT values will be close to uniform. We provide a histogram of these values for Model 3 in Appendix C, with equivalent plots for Models 0 to 5 being very similar. The histogram has a peak in the middle, suggesting that the posterior predictive densities for single observations are generally too “flat”, but the variability in the posterior predictive distributions is very small and therefore this does not cause too much concern about the model fit. If the PIT values concentrated strongly at 0 and 1, this would indicate that posterior predictive distributions would not allow for enough uncertainty, i.e., the model would be overconfident with its predictions; however, this is not the case here. We refer the reader to [Czado et al. \(2009\)](#) for more background on PITs. Due to the smoothness of our data we essentially have perfect predictions using Models 0 to 5, and these plots are not particularly informative, but again may be useful in settings where spatio-temporal interpolation is a modeling goal.

We also consider using a further cross validation procedure to compare the different models. This involves removing all data for locations lying in a quadrant to the south-east of the conditioning site, and using our methods to estimate these values. The difference between the estimates and original data, on the Laplace scale, can be summarized using the root mean square error (RMSE). These results are also provided in Table 1, where Model 3 gives the best results, although is only slightly favoured over the other Models 0 to 5.

3.7 Results for Model 3

For our application, it is difficult to distinguish between the performance of Models 0 to 5 using the cross validation approaches, but Models 3 and 4 both perform well in terms of the WAIC. We note that the run-time for Model 3, provided in Table 1, is less than one third of the run-time of Model 4 for this data, so we choose to focus on Model 3 here due to its simplicity. In general, simpler models have quicker computation times, but this is not necessarily always the case; we comment further on this in Section 4.3. We provide a summary of the fitted model parameters for Model 3, excluding the spline functions, in Table 2. The estimated value of σ^2 is very small, as expected. The Matérn covariance of the process $\{Z(s)\}$ has a reasonably large dependence range, estimated to be 428.2 km.

Parameter	Posterior mean	95% credible interval
σ^2	0.0107	(0.0106, 0.0107)
σ_Z	1.557	(1.496, 1.618)
ρ_Z	428.2	(409.5, 446.8)

Table 2: Estimated parameters for Model 3.

We now consider the estimated spline functions $\alpha(s - s_0)$ and $\gamma(s - s_0)$ for Model 3; these are shown in Figure 4. For comparison, we also show the estimate of $\alpha(s - s_0)$ for Model 1 and $\gamma(s - s_0)$ for Model 2. These two models

are similar to Model 3, in that $\beta = 0$, but $\gamma(s - s_0) = 0$ for Model 1 and $\alpha(s - s_0) = 1$ for Model 2, for all $s \in \mathcal{S}$. For Model 1, the $\alpha(s - s_0)$ spline function generally decreases monotonically with distance, as would be expected in spatial modeling. For Model 3, the interaction between the two spline functions makes this feature harder to assess, but further investigations have shown that although $\alpha(s - s_0)$ and $\gamma(s - s_0)$ are not monotonic in form, the combination $\alpha(s - s_0)x + \gamma(s - s_0)$ is usually decreasing for $x \geq u$; i.e., there is posterior negative correlation, and transfer of information between the two spline functions. Some examples of this are given in Figure 7 and will be discussed in Section 3.8. The behaviour of the $\gamma(s - s_0)$ spline function for Model 2 is similar to that of the $\alpha(s - s_0)$ functions for Models 1 and 3, highlighting that all three models are able to capture similar features of the data despite their different forms. The success of Model 3 over Models 1 and 2 can be attributed to the additional flexibility obtained via the inclusion of both spline functions. We note that in terms of representing the data, there may be little difference between suitable models, as we see here. However, we should also consider the diagnostics relating to our specific modeling purpose, which in our case is extrapolation. The results in Appendix A demonstrate that there is weakening dependence in the Red Sea data. The asymptotic dependence of Model 2 means that it cannot capture this feature, and is therefore unsuitable here.

Our fitted models can be used to obtain estimates of quantities relevant to the data application. For sea surface temperatures, we may be interested in the spatial extent of extreme events. High surface water temperatures can be an indicator of potentially damaging conditions for coral reefs, so it may be useful to determine how far-reaching such events could be. To consider such results, we fix the model hyperparameters and spline functions to their posterior means, and simulate directly from the spatial residual process of Model 3. If a thorough assessment of the uncertainty in these estimates was required, we could take repeated samples from the posterior distributions of the model parameters fixed to their posterior mean, and use each of these to simulate from the model. However, assessing the predictive distribution in this way is computationally more expensive, so we proceed without this step.

We separate the spatial domain into the 17 regions demonstrated in the left panel of Figure 5. Given that the value at the conditioning site exceeds the 0.95 quantile, we estimate the proportion of locations in each region that also exceed this quantile. Results obtained via 10,000 simulations from Model 3 are shown in the right panel of Figure 5, alongside empirical estimates from the data. These results suggest that Model 3 provides a successful fit of the extreme events, particularly within the first ten regions, which correspond to distances up to approximately 200 km from the conditioning site. At longer distances, the results are reasonably similar, and the difference may be due to the comparatively small number of locations that contribute to the model fit in these regions, and to some mild non-stationarities arising close to the coastline.

3.8 Sensitivity to the conditioning site

A natural question when applying the conditional approach to spatial extreme value modeling, is how to select the conditioning location. Under an assumption of spatial stationarity in the dependence structure, the parameters of the conditional model defined in (3) should be the same regardless of the location s_0 . However, since the data are used in slightly different ways for each conditioning site, and because the stationarity assumption is rarely perfect, we can expect some variation in parameter estimates for different choices of s_0 .

In Wadsworth and Tawn (2019) and Simpson and Wadsworth (2021), this issue was circumvented by using a composite likelihood that combined all possible individual likelihoods for each conditioning site, leading to estimation of a single set of parameters that reduced sampling variability and represented the data well on average. However, bootstrap methods are needed to assess parameter uncertainty, and as the composite likelihood is formed from the product of d full likelihoods, the approach scales poorly with the number of conditioning sites. Composite likelihoods do not tie in naturally to Bayesian inference as facilitated by the INLA framework, and so to keep the

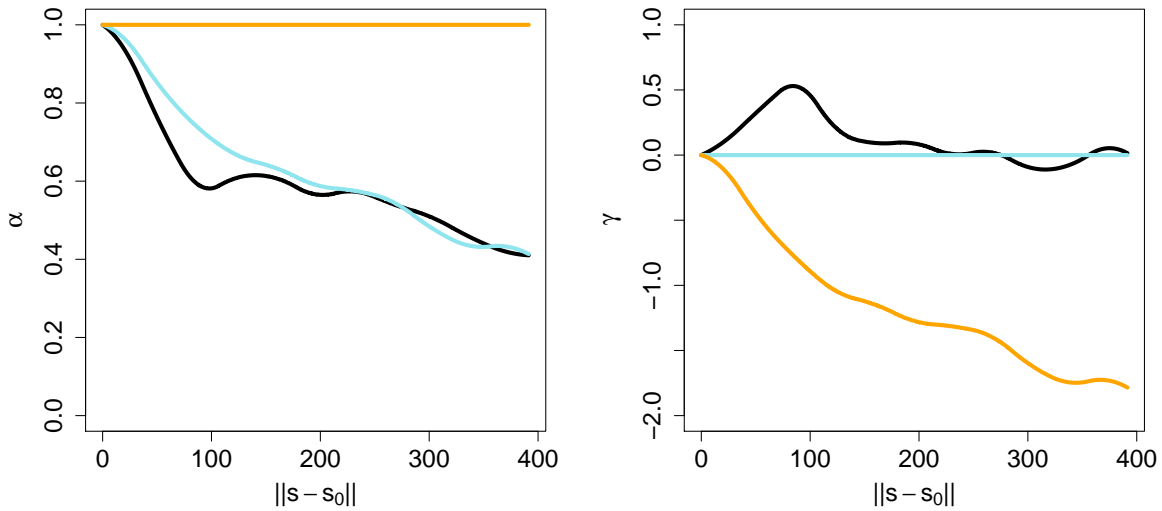


Figure 4: Posterior mean estimates of the spline functions $\alpha(s - s_0)$ (left) and $\gamma(s - s_0)$ (right) for Model 1 (blue), Model 2 (orange) and Model 3 (black).

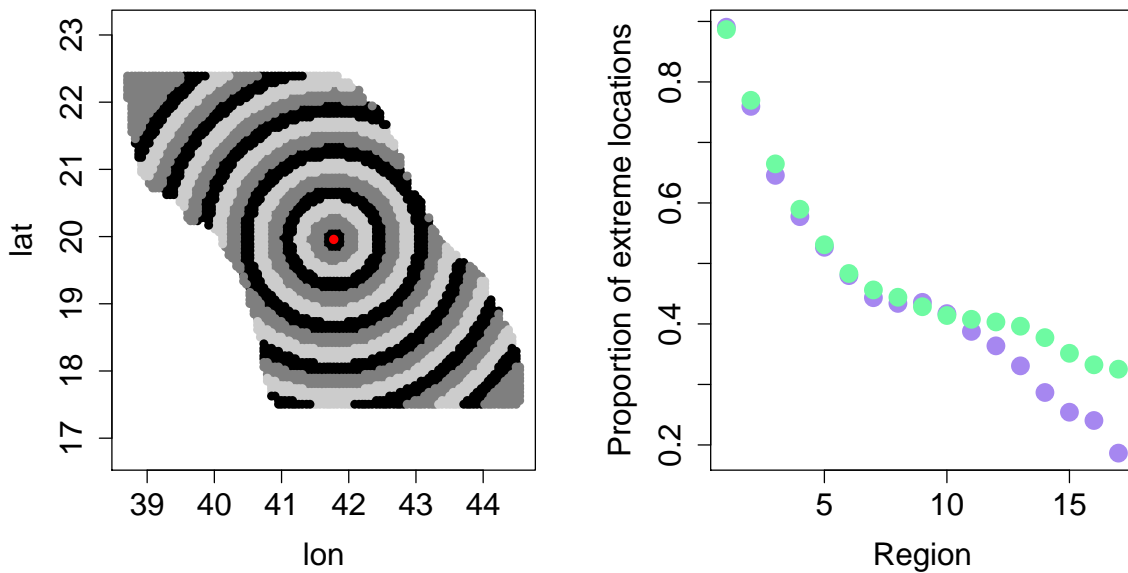


Figure 5: Left: the spatial domain separated into 17 regions; the region labels begin at 1 in the centre of the domain, and increase with distance from the centre. The conditioning site s_0 is shown in red. Right: the estimated proportion of locations that exceed the 0.95 quantile, given it is exceeded at s_0 using Model 3 (green) and equivalent empirical results (purple).

scalability, and straightforward interpretation of parameter uncertainty, we focus on implementations with a single conditioning location. Sensitivity to the particular location can be assessed similarly to other modeling choices, such as the threshold above which the model is fitted.

In particular, different conditioning sites may lead us to select different forms of the models described in Table 1, as well as the resulting parameter estimates. To assess this, we fit all seven models to the moderate dataset, using 39 different conditioning sites on a grid across the spatial domain, with the mesh and prior distributions selected as previously. We compare the models using the WAIC, as described in Section 3.5. The results are shown in Figure 6, where we demonstrate the best two models for each conditioning site. For the majority of cases, Model 4 performs the best in terms of the WAIC, and in fact, it is in the top two best-performing models for all conditioning sites. The best two performing models are either Models 3 and 4 or Models 4 and 5 for all conditioning locations. This demonstrates that there is reasonable agreement across the spatial domain, and suggests that using just one conditioning location should not cause an issue in terms of model selection.

To further consider how restrictive it is to only fit models at one conditioning site, we can compare the spline functions estimated using different locations for s_0 . We again focus on results for Model 3, as in Section 3.7, and consider estimates of $\alpha(s - s_0)u + \gamma(s - s_0)$, with u representing the threshold used for fitting. We demonstrate the estimates of this function in Figure 7, for the same 39 conditioning sites used in Figure 6, highlighting results for four of these sites situated across the spatial domain. Overall, the estimated functions are reasonably similar, particularly for shorter distances. There is one function that appears to be an outlier, corresponding to a conditioning site located on the coast. Although the other coastal conditioning sites we consider do not have this issue, it does suggest that some care should be taken here.

As a final test on the sensitivity to the conditioning site, we consider the implications if we fit Model 3 at one conditioning site, and use this for inference at another location. In particular, we take the results from Section 3.7, using a conditioning site near the centre of the spatial domain, and use these to make inference at a conditioning site located on the coast. We use a method analogous to the one used to create Figure 5. That is, we separate the spatial domain into regions, and for each one, we estimate the proportion of locations that take values above their 0.95 quantile, given that this quantile is exceeded at the conditioning location. In Figure 8, we compare results based on simulations from the fitted model to empirical estimates. Although a different conditioning location was used to obtain the model fit, the results are still good, particularly up to moderate distances, supporting our use of a single conditioning site for inference. One issue that is highlighted here is that by fitting the model at a central conditioning site, the maximum distance to s_0 is around 391 km, so we are not able to make inference about the full domain for a conditioning site near the boundary, where the maximum distance to other locations is much larger. This aspect should be taken into account when choosing a conditioning site for inference. This issue is specific to the use of spline functions for $\alpha(s - s_0)$ and $\gamma(s - s_0)$, and there is no such problem for parametric functions such as the one proposed by Wadsworth and Tawn (2019) for $\alpha(s - s_0)$. There is therefore a trade-off here between the flexibility of the splines and the spatial extrapolation possible using parametric functions.

4 Inference for conditional space-time extremes

4.1 Conditional spatio-temporal extremes models

Simpson and Wadsworth (2021) extend assumption (2) to a spatio-temporal setting. The aim is to model the stationary process $\{X(s, t) : (s, t) \in \mathcal{S} \times \mathcal{T}\}$ which also has marginal distributions with exponential upper tails. The conditioning site is now taken to be a single observed space-time location (s_0, t_0) , and the model is constructed for a finite number of points $(s_1, t_1), (s_1, t_2), \dots, (s_d, t_\ell)$ pertaining to the process at d spatial locations and ℓ points

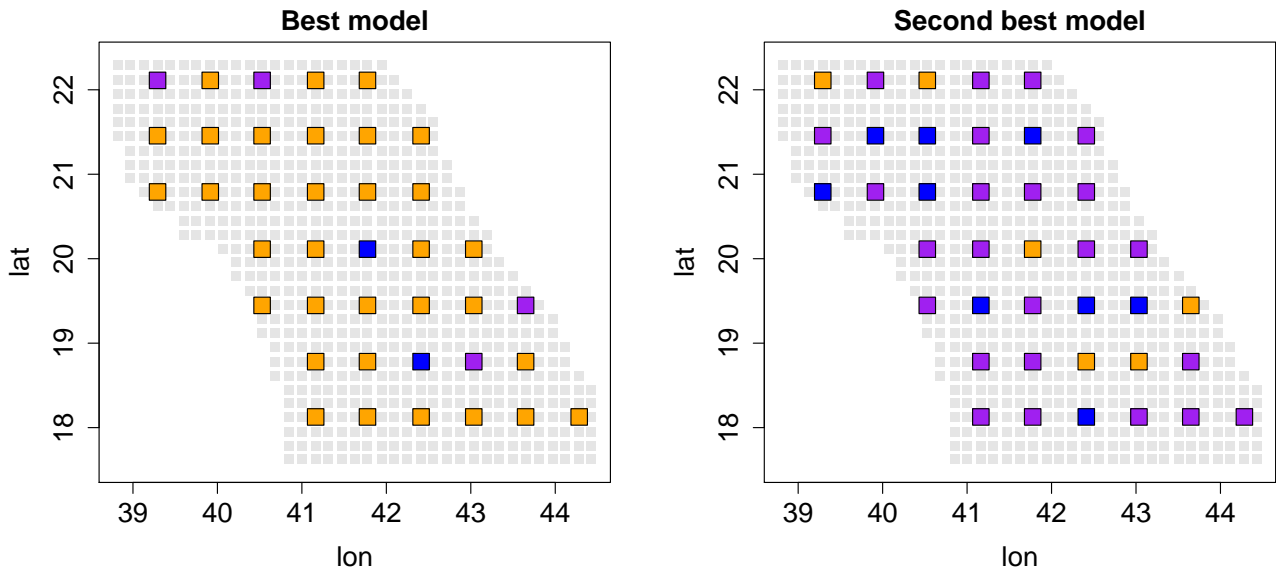


Figure 6: Maps showing the ‘best’ and ‘second best’ models using different conditioning sites, based on minimizing the WAIC: Model 3, blue; Model 4, orange; Model 5, purple.

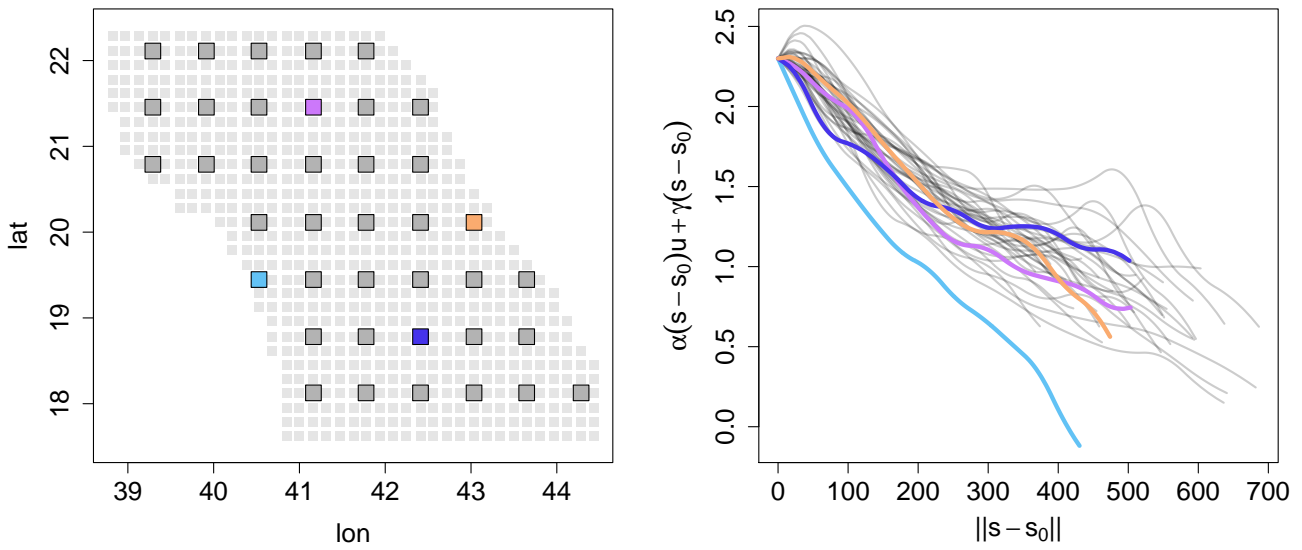


Figure 7: The estimated value of $\alpha(s - s_0)u + \gamma(s - s_0)$ for Model 3 (right), with u representing the threshold used in the model fits. The colours of the lines correspond to the conditioning sites used, as shown in the left panel.

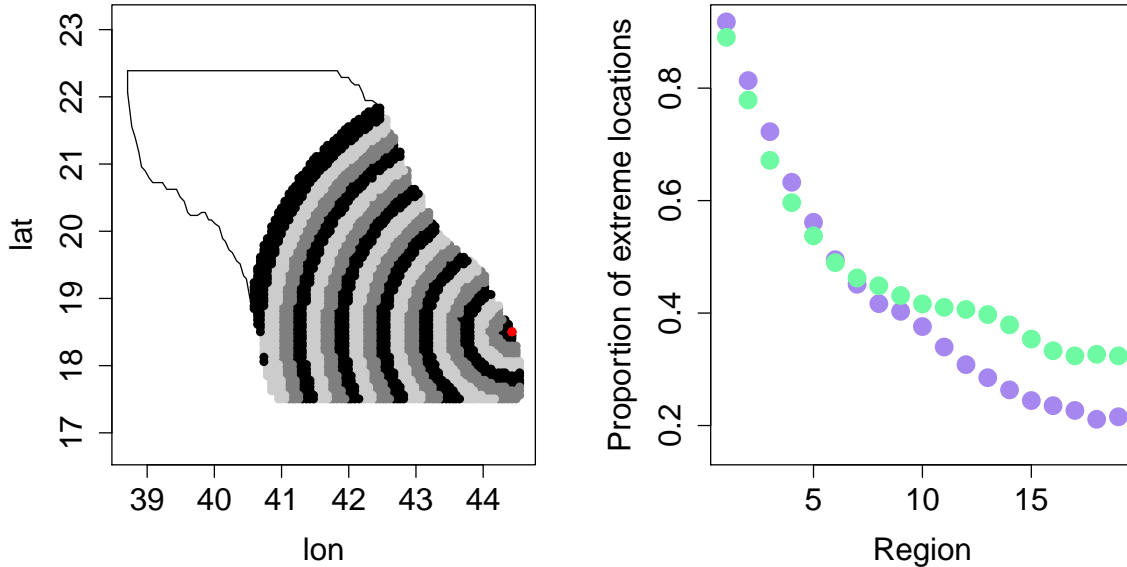


Figure 8: Left: the spatial domain separated into regions; the region labels begin at 1 at s_0 (red), and increase with distance from this location. Right: the estimated proportion of locations that exceeded the 0.95 quantile, given it is exceeded at s_0 using Model 3 (green) and equivalent empirical results (purple).

in time, where data may be missing for some of the space-time points. The structure of the conditional extremes assumption is very similar to the spatial case, in particular, it is assumed that there exist functions $a_{(s,t)-(s_0,t_0)}(\cdot)$ and $b_{(s,t)-(s_0,t_0)}(\cdot)$ such that as $u \rightarrow \infty$,

$$\Pr \left(\left[\frac{X(s_i, t_j) - a_{(s_i, t_j)-(s_0, t_0)} \{X(s_0, t_0)\}}{b_{(s_i, t_j)-(s_0, t_0)} \{X(s_0, t_0)\}} \right]_{\substack{i=1, \dots, d, \\ j=1, \dots, \ell}} \leq \mathbf{z} \mid X(s_0, t_0) = u \right) \rightarrow \Pr \left[\{Z^0(s_i, t_j)\}_{\substack{i=1, \dots, d, \\ j=1, \dots, \ell}} \leq \mathbf{z} \right],$$

for a spatio-temporal residual process $\{Z^0(s, t)\}$. Once more the excesses $X(s_0, t_0) - u \mid X(s_0, t_0) > u$ are independent of the residual process as $u \rightarrow \infty$, and the constraints on the residual process $\{Z^0(s, t)\}$ and normalizing function $a_{(s,t)-(s_0,t_0)}(\cdot)$ are analogous to the spatial case. We consider spatio-temporal variants of spatial models 1, 3, 4 and 5, which provided the best WAIC values, in Section 3.3; see the model summary in Table 3. In order to preserve sparsity in the precision matrix, a simple autoregressive structure is employed for the temporal aspect of the residual process; further details are provided in Section 5.5. Specifically, we construct the process $\{Z^0(s, t)\}$ as $\{Z(s, t)\} - Z(s_0, t_0)$ using the first-order autoregressive structure in combination with the 2D spatial SPDE model as described in equation (8). Similarly, the prior distributions for $\alpha(s - s_0, t - t_0)$ and $\gamma(s - s_0, t - t_0)$ are constructed according to (8), with a 1D SPDE model for a quadratic spline with 14 interior knots deployed for spatial distance; these Gaussian prior processes are conditioned to have $\alpha(0, 0) = 1$ and $\gamma(0, 0) = 0$.

4.2 Spatio-temporal Red Sea surface temperature data

Since the spatio-temporal models are more computationally intensive than their spatial counterparts due to a larger number of hyperparameters and more complex precision matrices, we focus only on the moderate set of spatial locations demonstrated in Figure 2, which contains 678 spatial locations; this will still result in a substantial number of dimensions when we also take the temporal aspect into account.

To carry out inference for the conditional spatio-temporal model, we separate the data into temporal blocks of equal length, with the aim that each block corresponds to an independent observation from the process $\{X(s, t)\}$. We apply a version of the runs method of [Smith and Weissman \(1994\)](#) to decluster the data into blocks of seven days. The declustering is applied only with respect to the spatial conditioning site s_0 , but we still consider observations across all spatial locations at the corresponding time-points. Explicitly, we consider exceedances of our chosen threshold u at s_0 ; as we move forwards in time from the start of the data, the first exceedance of the threshold becomes the start of the first block, with the following six days making up the rest of the block; we then continue to move forwards in time until we have seen at least r non-exceedances of u at s_0 , and the next exceedance becomes the start of the next block; the process continues until we reach the end of our observation period. We fix the tuning parameter in the runs method to $r = 12$, and note that since we focus only on summer months, blocks should not be allowed to span multiple years. This declustering approach yields 28 blocks of seven days to which we can apply our four spatio-temporal models.

4.3 Model selection, forecasting and cross validation

We compare the four models using similar criteria as in the spatial case. The WAIC and average CPO values are presented in [Table 3](#), where the most complex Model 4 performs best in terms of the WAIC, while a slightly better CPO value arises for Model 3. We note that the model selected using the WAIC has the same form in both the spatial and spatio-temporal cases.

We also compare fitted and observed values using a variant of the root mean square error (RMSE). The results of within-sample RMSEs are almost identical for the four models, and therefore not included in [Table 3](#), yielding a value of 0.077. To assess predictive performance, it is more interesting to consider an additional variant of cross validation in the spatio-temporal case to test the forecasting ability of the models. We carry out seven-fold cross validation by randomly separating our 28 declustered blocks into groups of four, and for each of these groups we remove the observations at all locations for days two to seven. We then fit the model using the remaining data in each case, and obtain predictions for the data that have been removed. This cross validation procedure is straightforward to implement, as in R-INLA it is possible to obtain predictions (e.g., posterior predictive means), including for time-points or spatial locations without observations. We compare the predicted values with the observations that were previously removed, presenting the cross validation root mean square error (RMSE_{CV}) in [Table 3](#). Again, the results are quite similar, but Model 3 performs slightly better than the others. Finally, run-times are reported in the table and range between 1 hour and 4 hours, using 2 cores on machines with 32Gb of memory. When comparing the spatial models with the corresponding space-time models having the same spatial component, the order of run-times changes in our results. We emphasize that, on average, more complex latent models will require longer run-times with INLA if the observations remain the same. However, the Laplace approximations conducted by INLA require iterative optimization steps to find modes of high-dimensional functions, and in some cases these optimization steps may be substantially more computer-intensive for a simpler model, for instance when the mode is relatively hard to identify. Therefore, there is no contradiction in the reported results.

5 Computational and implementation details

5.1 Introduction

This section provides further details on INLA, the SPDE approach, and specifics of implementation that are necessary to gain a full understanding of our methods, but not to appreciate the general ideas behind the approach.

Model number	Model form	WAIC	CPO	RMSE _{CV}	Run-time
1	$x \cdot \alpha(s - s_0, t - t_0) + \{Z^0(s, t)\}$	108	-0.0003	0.001	99
3	$x \cdot \alpha(s - s_0, t - t_0) + \gamma(s - s_0, t - t_0) + \{Z^0(s, t)\}$	59	0	0	206
4	$x \cdot \alpha(s - s_0, t - t_0) + \gamma(s - s_0, t - t_0) + x^\beta \cdot \{Z^0(s, t)\}$	0	-0.0018	0.091	71
5	$x \cdot \alpha(s - s_0, t - t_0) + x^\beta \cdot \{Z^0(s, t)\}$	47	-0.0004	0.094	89

Table 3: Summary of conditional space-time models, model selection criteria, and total run-times (minutes). The minimum WAIC value (-215973 for Model 4); maximum CPO value (2.92 for Model 3); and minimum RMSE_{CV} value (1.09 for Model 3) have been subtracted from their respective columns. We estimate β as 0.55 with a 95% credible interval of (0.49, 0.64) (Model 4) and 0.55 (0.50, 0.65) (Model 5).

5.2 Bayesian inference with the integrated nested Laplace approximation

The integrated nested Laplace approximation (INLA [Rue et al., 2009, 2017](#); [Opitz, 2017](#); [van Niekerk et al., 2019](#)) provides relatively fast and accurate analytical approximations for posterior inference in models with latent Gaussian processes. The distribution of the observed variables may be non-Gaussian conditional on the latent Gaussian process, although here the focus of our modeling approach for conditional extremes is on Gaussian responses; this does not imply a joint Gaussian assumption on our data, as explained in [Section 1.3](#). The method astutely combines Laplace approximations ([Tierney and Kadane, 1986](#)), used to compute expectations with respect to high-dimensional multivariate Gauss–Markov random vectors (denoted by \mathbf{W} in [Section 2.1](#), with up to tens of thousands of components), with efficient numerical integration schemes for integration with respect to a relatively small number of hyperparameters (denoted by θ) governing variance and dependence of Gaussian components, and the shape of the distribution of observations. Therefore, it bypasses issues that may arise with simulation-based Markov chain Monte Carlo (MCMC) inference, where the design of stable algorithms for fast exploration of the posterior distribution may be hampered by intricate dependencies between the components of the model (e.g., [Rue and Held, 2005](#)). INLA is implemented in the INLA package ([Lindgren and Rue, 2015](#)) of the R statistical software, also referred to as R-INLA, and over the last decade it has been widely adopted for Bayesian additive regression modeling of spatial and spatio-temporal data due to its integration with the stochastic partial differential equation (SPDE) approach ([Lindgren et al., 2011](#); [Krainski et al., 2018](#)), which provides convenient Gauss–Markov approximations to the Matérn covariance function. The Bayesian framework of INLA allows for joint estimation and uncertainty assessment of latent components, hyperparameters and predictions. Recently, the speed and stability of INLA with high-dimensional latent Gaussian structures were further leveraged through its integration with the sparse matrix computation library PARDISO ([van Niekerk et al., 2019](#)).

5.3 The SPDE approach

The latent variable framework allows us to choose the spatial resolution of the latent model separately from that of the observed locations. Moreover, we can use the results of [Lindgren et al. \(2011\)](#), known as the stochastic partial differential equation (SPDE) approach, to work with numerically convenient Markovian approximations to the Matérn covariance function, leading to sparse precision matrices. We consider random fields defined on \mathbb{R}^D ; for the residual process $\{Z^0(s)\}$, $D = 2$, but we will also use this framework with $D = 1$ to define the spline functions with respect to the distance to the conditioning site. The SPDE is given by

$$(\kappa^2 - \Delta)^{\zeta/2} \tau\{Z(s) : s \in \mathbb{R}^D\} = \{B(s) : s \in \mathbb{R}^D\}, \quad \zeta = \nu + D/2, \quad (6)$$

with the Laplace operator $\Delta y = \sum_{j=1}^D \partial^2 y / \partial^2 x_j$, a standard Gaussian white noise process $\{B(s)\}$, and parameters $\kappa > 0$ (controlling correlation range) and $\tau > 0$ (controlling the variance). It has a unique stationary solution given by a zero-mean Gaussian process $\{Z(s)\}$ with Matérn covariance function. Here, ν is the shape parameter of the Matérn, with $\nu = 0.5$ yielding the exponential covariance model. The marginal variance is $\Gamma(\nu)/(\Gamma(\nu + D/2)(4\pi)^{D/2}\kappa^{2\nu}\tau^2)$, and the *empirical range*, where a correlation of approximately 0.1 is attained between two points, is approximately $\sqrt{8\nu}/\kappa^2$. Note that this range parameter is different from the range in the classical Matérn parametrization.

In practice, the domain is finite, i.e., different from \mathbb{R}^D , and appropriate boundary conditions must be imposed to ensure a solution that is unique in terms of finite-dimensional distributions. An approximation to the exact solution satisfying the boundary conditions is constructed through the representation $Z(s) = \sum_{j=1}^m W_j \Psi_j(s)$ with locally supported basis functions $\Psi_j(s)$ (e.g., linear or quadratic B-splines for $D = 1$, and finite elements for $D = 2$). The basis functions do not depend on SPDE parameters. The stochastic solution $\{Z(s)\}$ of the SPDE in the subspace of functions spanned by the linear combination of basis functions then yields $\mathbf{W} = (W_1, \dots, W_m)^T \sim \mathcal{N}_m(0, Q^{-1})$ with precision matrix Q known in analytical form. We emphasize that $\{Z(s)\}$ here could represent the splines used for $\alpha(s - s_0)$ or $\gamma(s - s_0)$, or the spatial process used in the construction of $\{Z^0(s)\}$. In Section 2.2, we labelled the corresponding latent variables $\mathbf{W}_\alpha \in \mathbb{R}^{m_\alpha}$, $\mathbf{W}_\gamma \in \mathbb{R}^{m_\gamma}$ and $\tilde{\mathbf{Z}}^0 \in \mathbb{R}^{m_z}$. For $D = 2$, we use Neumann boundary conditions where the outward derivative of the realizations of the Gaussian field is zero, which is the default choice for spatial modeling with INLA. For $D = 1$ and a support given by an interval, a unique approximation to the SPDE solution exists with free boundaries. In our models where spline functions are constrained to value zero at the origin, we use constructions with a Dirichlet boundary on the left side of the interval, such that the solution satisfies the constraint. Theoretical results in Lindgren et al. (2011) show that the approximation to the solution is good in general and can be made arbitrarily close by choosing a finer finite element mesh.

The value of ζ in (6) determines how the approximate solution of the SPDE can be constructed in practice (Lindgren et al., 2011), and it must be fixed when estimating the model with INLA. The INLA implementation currently supports using $\zeta \in [1, 2]$, i.e., $\nu \in [0, 1]$ for $D = 2$.

The vector $\tilde{\mathbf{Z}}^0$ contains the variables used to represent a single replicate of the Gaussian process. When modeling conditional extremes, we usually extract $n > 1$ extreme episodes satisfying $X(s_0) > u$. To represent the unconstrained residual spatial process $\{Z(s)\}$, we therefore need independent replicates $\tilde{\mathbf{Z}}_j^0$, $j = 1, \dots, n$, of $\tilde{\mathbf{Z}}^0$. Moreover, for the purpose of space-time modeling, we may assume that single episodes span $\ell \geq 1$ time steps. Then, for the unconstrained residual process $\{Z(s)\}$ associated with each episode, we will define a Gaussian vector with $\ell \times m_z$ components, and there will be n replicates of this vector. We will write the precision matrices of Gaussian vectors comprising several blocks of the initial variables $\tilde{\mathbf{Z}}^0$ through Kronecker products of matrices; see Section 5.5.

5.4 Imposing the condition $Z^0(s_0) = 0$ on the residual process

As mentioned in Section 1.2, the residual process $\{Z^0(s)\}$ in the spatial conditional extremes model can be constructed by starting with a Gaussian process $\{Z(s)\}$ and imposing the $(Z(s_0) = 0)$ -constraint in some way. Wadsworth and Tawn (2019) propose two options: either subtract the value at the conditioning site, i.e., set the residual process to be $\{Z(s)\} - Z(s_0)$; or use the conditional process $\{Z(s)\} | Z(s_0) = 0$.

In the latent variable framework, we can obtain a residual process of form $\{Z(s)\} - Z(s_0)$ without losing the latent Markovian structure, since we only need to manipulate the representation for $\{Z(s)\}$, which has a sparse precision matrix. The latent variables representing $\{Z(s)\}$ are handled as usual, but we modify the observation matrix A_S of the spatial process $\{Z(s)\}$ to obtain A_S^0 , the observation matrix associated with the process $\{Z(s)\} - Z(s_0)$.

Therefore, let A_{s_0} denote the observation matrix for the conditioning site of dimension $1 \times m_Z$, and A_S the observation matrix for the observation locations with dimension $d \times m_Z$. Then, we apply the transformation

$$A_S^0 = A_S - \begin{pmatrix} A_{s_0} \\ \vdots \\ A_{s_0} \end{pmatrix} \in \mathbb{R}^{d \times m_Z} \quad (7)$$

to obtain the new observation matrix.

The alternative approach is to impose the $(Z(s_0) = 0)$ -constraint via conditioning, in the sense of the conditional probability distribution. In general, if $\mathbf{W} \sim \mathcal{N}_m(\mathbf{0}, Q^{-1})$ is an m -dimensional Gaussian random vector with precision matrix Q , we may want to impose a linear constraint of the form

$$B\mathbf{W} = \mathbf{e}, \quad B \in \mathbb{R}^{k \times m}, \quad \mathbf{e} \in \mathbb{R}^k,$$

where k is small. For instance, $B = (1, 0, \dots, 0)$ and $\mathbf{e} = 0$ if we constrain the Gaussian vector to satisfy $W_1 = 0$, or $B = (1/m, \dots, 1/m)$ and $\mathbf{e} = 0$ if we constrain the average value to 0. The linear transformation

$$\mathbf{W} \mid (B\mathbf{W} = \mathbf{e}) \stackrel{d}{=} \mathbf{W} - Q^{-1}B^T (BQ^{-1}B^T)^{-1} (B\mathbf{W} - \mathbf{e})$$

of the unconstrained vector \mathbf{W} imposes this constraint in the sense of generating a realization of the conditional distribution given $B\mathbf{W} = \mathbf{e}$. In practice, one can calculate BQ^{-1} by solving k linear systems without explicitly calculating and storing Q^{-1} , and fast implementations exist when Q is sparse and k is very small. This approach is known as *conditioning by kriging* (see, e.g., equation (8) in [Rue et al., 2009](#); [Cressie, 1993](#)); it is available in R-INLA, and we use it for the implementation of the models presented here. Another possibility, applicable in a more specific setting by allowing us to directly condition the Gaussian vector \mathbf{W} on $W_1 = 0$ (here using the first component without loss of generality), is to remove W_1 from \mathbf{W} , resulting in \mathbf{W}_{-1} . The precision matrix of \mathbf{W}_{-1} conditional on $W_1 = 0$ then corresponds to Q but with the first row and the first column removed. Since this approach is less general (specifically, in order to impose $Z^0(s_0) = 0$, we require that a knot is placed at s_0), we here prefer the approach of conditioning through kriging. With respect to model structure, the difference between the two approaches is that conditioning through kriging does not fix the constraint in the prior model, but imposes it in the posterior model by applying the conditioning transformation during the Laplace approximations of INLA, while the second approach directly fixes the constraint in the prior model. In both cases, the condition is appropriately incorporated into the posterior model, and no notable differences arise in the posterior models returned by R-INLA.

For our Red Sea data application, we found that the choice of residual process does not have a large impact on results. The option of using the form $\{Z(s)\} - Z(s_0)$ performed slightly better overall, and we therefore used this method for the results presented in Sections 3 and 4. A comparison of results using the two different approaches is provided in Appendix B.1.

5.5 Space-time Gauss-Markov models

Inference on spatial conditional extremes is usually based on replicated observations, corresponding to extreme events of the spatial process $\{X(s)\}$, and in the case of space-time conditional extremes on replicated observations of extreme episodes stretching over several time steps. In this subsection, we detail how to combine Kronecker products of precision matrices, appropriate observation matrices, and the conditioning approaches outlined in Section 5.4, to generate the latent variable representations of the residual processes $\{Z^0(s)\}$ using sparse precision matrices.

residual process $\{Z^0(s, t)\} = \{Z(s, t)\} - Z(s_0, t_0)$ is given by the modified block-diagonal matrix

$$A_{ST}^0 = \begin{pmatrix} A_S & 0 & \cdots & \cdots & 0 \\ 0 & A_S & 0 & \cdots & 0 \\ \vdots & \ddots & \ddots & \ddots & \vdots \\ 0 & \cdots & 0 & A_S & 0 \\ 0 & \cdots & \cdots & 0 & A_S \end{pmatrix} - \begin{pmatrix} A_{s_0, t_0} \\ \vdots \\ \vdots \\ \vdots \\ A_{s_0, t_0} \end{pmatrix},$$

with ℓ blocks on the diagonal, and one or several columns with the same non-negative entries for all rows to represent the term $-Z(s_0, t_0)$. Then, the representation A_{ST}^0 coincides with A_S^0 in the case of purely spatial extreme episodes ($\ell = 1$).

Finally, we take into account the replication structure with n observed replicates of extreme spatial or spatio-temporal episodes. By assuming that each replicate has the same design of spatial locations observed over ℓ time steps, we can write the overall observation matrix as the Kronecker product $A_{\text{repl}} = I_n \otimes A_{ST}^0$ with the $n \times n$ identity matrix I_n .

We emphasize that we use the constructions of spatio-temporal processes based on (8) for two purposes. First, we can specify the residual process $\{Z^0(s, t)\}$ by using $\{Z^0(s)\}$, with $s \in \mathcal{S} \subset \mathbb{R}^2$, in (8). Second, we can model the function $a_{(s,t)-(s_0,t_0)}$, by using a_{s-s_0} in (8). The latter case can be seen as the use of a Gaussian process prior for the coefficients of a tensor product spline basis, defined with respect to the dimensions of spatial distance and time lag.

The form of the process $\{Z(s, t)\}$ used here exhibits separability in space and time. At present, there are no other, more flexible non-separable models indexed over continuous space and readily implemented within R-INLA, although the possibility of such models has been discussed by Bakka et al. (2018). Simpson and Wadsworth (2021) consider the case for using a non-separable form of $\{Z(s, t)\}$ within spatio-temporal conditional extremes models. They conclude that allowing for non-separability in the normalizing functions is more important since these capture more of the structure in the model. Within R-INLA, the semiparametric specification of the first normalizing function $a_{(s,t)-(s_0,t_0)}$ allows for flexible, non-separable structure in the posterior estimate of the function. More complex, non-separable parametric forms of the function $b_{(s,t)-(s_0,t_0)}$ could be estimated by analogy with the spatial case, so using a separable form of $\{Z(s, t)\}$ here should be sufficient.

5.6 Implementation using the R-INLA software

While standard functionality available in the R-INLA library allows for straightforward implementation of the unconstrained SPDE model and auto-regressive structures for dimensions $D = 1, 2$, as presented in Sections 5.3 and 5.5, respectively, more specific extensions are required for imposing the condition $Z^0(s_0, t_0) = 0$.

The R-INLA package provides the precision matrices of the unconstrained latent spatial process $\{Z(s)\}$. Space-time processes $\{Z(s, t)\}$, and independent replications of spatial or spatio-temporal processes, are then handled internally by R-INLA. To estimate model components of type $b_{(s,t)-(s_0,t_0)}(x) [\{Z(s, t)\} - Z(s_0, t_0)]$, with a deterministic function $b_{(s,t)-(s_0,t_0)}$ that contains no parameters to be estimated through INLA, we can then simply modify the observation matrix A_{repl} and give it as input to the estimation routine. As to imposing the constraint where we condition on $Z(s_0, t_0) = 0$, the conditioning-by-kriging approach using a matrix B and a vector e is already implemented for the spatial $\{Z(s)\}$ process ($D = 2$), and can be used for spatial extreme episodes with $\ell = 1$. Similarly, for $D = 1$ the condition $Z(0) = 0$ can be set through a flag in R-INLA, and we will deploy this mechanism to constrain priors of spline functions used to model the functions $\alpha(s - s_0)$ and $\gamma(s - s_0)$ in (5). However, space-time models ($\ell > 1$) with temporal auto-regression, where the condition is active only for exactly

one of the ℓ time steps, are not possible through this mechanism in R-INLA. Similarly, variances of the residual space-time process $b_{(s,t)-(s_0,t_0)}(x)\{Z^0(s,t)\}$ that vary over the ℓ time steps, with non-stationary expressed through hyperparameters to be estimated, are not directly available.

Many additive components of the latent model that are not directly available through standard mechanisms in R-INLA can be implemented manually through its `rgeneric` function. This requires us to manually define functions that return the precision matrix, the (deterministic) mean function (if different from 0), and the prior densities of the hyperparameters of the component to be set up. In particular, the function $b_{(s,t)-(s_0,t_0)}(x)$ may depend on hyperparameters to be estimated. Moreover, we could estimate a parametric mean function $a_{(s,t)-(s_0,t_0)}(x)$ in $a_{(s,t)-(s_0,t_0)}(x) + b_{(s,t)-(s_0,t_0)}(x)\{Z^0(s,t)\}$, where $a_{(s,t)-(s_0,t_0)}(x)$ depends on hyperparameters but does not involve any of the latent Gaussian components gathered in the vector \mathbf{W} . Finally, the conditioning on $Z(s_0, t_0) = 0$ in the spatio-temporal setting ($\ell > 1$) can be imposed by combining an unconditional `rgeneric`-model with the conditioning through kriging technique available as a standard mechanism within R-INLA. In all operations involving large precision matrices, it is crucial to use appropriate sparse matrix objects and sparse matrix operations in the R language.

In Section 3.6, we proposed a cross validation procedure that involved removing and subsequently predicting observations in a particular region of the spatial domain. We now highlight that in R-INLA, this is straightforward to achieve by replacing the data for the cross validation by missing data flags, since these values will automatically be estimated, e.g., through the posterior mean of the “fitted values”.

We note that some potentially useful constructions are not possible with R-INLA because they violate the linear structure in the Gaussian predictor vector $\boldsymbol{\eta}$ as expressed through the latent Gaussian components of \mathbf{W} . For instance, suppose we wish to construct a prior distribution for a term of the right-hand side in (5) as follows: $h(A_1\mathbf{W}_1) \times A_2\mathbf{W}_2$, with $A_2\mathbf{W}_2$ corresponding to the spatial residual process $\{Z^0(s)\}$ in equation (4), and $A_1\mathbf{W}_1$ a Gaussian process prior for a spline function ($D = 1$) where an (arbitrary) function h is used to specify the scale function $b_{s-s_0}(x)$. This construction involves a non-linear combination of the latent Gaussian components \mathbf{W}_1 and \mathbf{W}_2 , which is not possible.

6 Discussion

The aim of this paper was to develop an inferential approach for spatial and spatio-temporal conditional extremes models, by exploiting latent Gaussian processes within the SPDE framework, and with efficient inference carried out using R-INLA. A benefit of this method is that we are able to handle more spatial or spatio-temporal locations than is possible using existing likelihood-based techniques. In principle, the Laplace approximations carried out within INLA could also be used for frequentist inference without specifying prior distributions for hyperparameters, but we emphasize that the Bayesian framework comes with some valuable benefits, such as the control of model complexity via the use of penalized complexity priors. High-dimensional inference was facilitated by accepting some modest restrictions on the modeling set up. Firstly, we only considered inference based on a single conditioning location. As mentioned in Section 3.8, in other contexts sensitivity to the choice of conditioning location has been reduced by use of composite likelihoods to incorporate all potential conditioning locations. However, this comes at a computational cost, with a further much larger cost to assess uncertainty via the bootstrap. Secondly, we only allow for the residual process to have a Gaussian form. In many applications this is likely to be adequate, but may lead to problems if the domain of the data is sufficiently large that there is approximate independence in the extremes at long distances. This is because under independence, we expect $\alpha(s - s_0) = 0$, $\gamma(s - s_0) = 0$ and $\beta = 0$, such that $\{X(s)|[X(s_0) = x]\} = \{Z^0(s)\}$, but there is a mismatch between the marginals of $\{X(s)\}$

(Laplace) and $\{Z^0(s)\}$ (Gaussian). [Wadsworth and Tawn \(2019\)](#) dealt with this by allowing more general forms for the margins of $\{Z^0(s)\}$, but where this is not necessary, use of untransformed Gaussian processes is certainly more efficient. In principle, non-Gaussian responses can be handled within R-INLA by using a response distribution (i.e., a “likelihood model”) different from the Gaussian; however, due to the conditional independence assumption with respect to the latent Gaussian process, it may be difficult to obtain models that realistically reflect the spatio-temporal smoothness of observations. In contrast to the existing inferential approach, INLA allows us to estimate flexible semiparametric specifications for the functions arising in the mean of the Gaussian process of conditional extremes, and the estimation and uncertainty assessment is performed jointly with all other model parameters.

Since we construct models using a single conditioning site, s_0 , but may subsequently assume that the fitted model applies at other conditioning locations, another important consideration is the choice of a suitable position for s_0 . There are certain aspects to take into account here, as highlighted in [Section 3.8](#). For instance, one may wish to choose s_0 so that $\max_{i=1,\dots,d} \|s_i - s_0\|$ takes its largest value, as this will provide more reliable estimates for the spline functions $\alpha(s - s_0)$ and $\gamma(s - s_0)$ at the longest distances. On the other hand, choosing s_0 towards the edge of the spatial domain may mean that it is less likely to be representative of the full set of locations. These two considerations should be balanced in the selection of s_0 . Even when inference on parameters has been made using a single conditioning location, our assumption of spatial stationarity means that it is still possible to infer conditional probabilities or expectations for alternative conditioning sites or events. In particular, [Wadsworth and Tawn \(2019\)](#) demonstrate how to make inference on quantities of the form

$$E[g(\{X(s)\}) | \max_{1 \leq i \leq d} X(s_i) > u],$$

for a function $g(\cdot)$ of interest, which could be exploited in our setting just as easily.

In other application contexts, the analysis of non-stationarities in conditional extremes with respect to s_0 may be of interest, such that the assessment of differences between models fitted at different conditioning locations s_0 is an inferential goal in itself. The local modeling suggested by the conditional extremes approach makes sense if we have a large study area with possible non-stationarities, but are mostly interested in inferences on local features. For example, with the Red Sea surface temperature data, one could choose s_0 as a representative site of one coral reef, or several closely located coral reefs, although we have not done this here. In climate studies, loosely speaking “climate” is often considered as pertaining to the characteristics of the marginal distribution, while “weather” is additionally driven by the local spatio-temporal dependence; with the conditional extremes models, we could also consider the properties of the s_0 -conditioned model as part of the “climate” at s_0 .

As discussed in [Section 3.8](#), [Wadsworth and Tawn \(2019\)](#) and [Simpson and Wadsworth \(2021\)](#) use a composite likelihood approach to combine information across several conditioning sites. While this is also a possibility in our setting, we would lose some of the benefits over the classical likelihood framework since the uncertainty estimation becomes awkward in a Bayesian context, though consistency of estimators is preserved ([Soubeyrand and Haon-Lasportes, 2015](#)). An alternative may be to obtain separate estimates for different conditioning locations, and combine these via some weighted approach, i.e., perform model averaging either in the domain of the models’ likelihood or in the domain of their predictions. This provides a potential avenue for further work.

While this was not necessary for our Red Sea data example, it would be relatively straightforward to include covariates within the latent Gaussian structure. For instance, a distant-dependent variance model may be more appropriate in certain cases, and such an adaptation would be possible within the INLA framework by suitable modification of the models outlined in [Table 1](#). As is generally the case with covariate modeling, the difficulty here is in choosing relevant covariates whose influence can be easily interpreted. For some scenarios, the effect of a particular covariate may already be known, and the modeling may benefit from this approach. Another technique that may be useful in certain settings is censoring, which is also possible within the INLA framework via the

inclusion of a censored Gaussian response for the likelihood of observations in Section 2.1; see Zhang et al. (2021) for an MCMC-implementation in a similar context.

A further issue linked to modeling non-stationarity is the assumption of isotropy that we place on the underlying spatial process. Indeed, the results in Appendix A show that there is some violation of this assumption in our application. Wadsworth and Tawn (2019) deal with anisotropy by including a transformation of the spatial coordinates within the modeling procedure. This approach is also adopted by Simpson and Wadsworth (2021), and the resulting transformation for the sea surface temperature data in the northern Red Sea is very small. Such a transformation is not incorporated within the standard R-INLA set-up, but the anisotropy parameters could be estimated using a generic model. In the spatial setting, Richards and Wadsworth (2021) propose a deformation technique to deal with non-stationarity in extremal dependence features. This allows for anisotropy to be handled as a preliminary modeling step, which it would be possible to do in the context of conditional spatial extremes.

Our approach is not fully Bayesian, since the marginal transformation of data at each spatial location to a standard Laplace distribution is carried out separately to the dependence modeling. This approach appears sufficient, particularly since simultaneous estimation of the margins and the dependence within the INLA framework would be intricate. This would result in us resorting to MCMC estimation, but here we do not want to sacrifice the simplicity and speed of the INLA-implementation with big datasets.

There are several aspects that we have had to consider as part of the implementation of the conditional extremes models in INLA, with some of these being more important than others. We found the priors of the hyperparameters to have minimal importance, as indicated by posteriors with small credible intervals. This is likely due to the large number of observations we had available. We also observed very similar results when setting the SPDE parameter to $\zeta = 1.5$ or $\zeta = 2$, so for our data, the smoothness of the Gaussian field does not have a significant impact compared to other aspects of the model. As we may have expected, choosing appropriate normalizing functions is hugely important, and the forms of these may need to be tailored to the specific data application.

Data and code Code to implement the models in this paper is available online in the GitHub repository <https://github.com/essimpson/INLA-conditional-extremes>, and the sea surface temperature data can be downloaded at <https://marine.copernicus.eu>.

References

- Bakka, H., Rue, H., Fuglstad, G.-A., Riebler, A., Bolin, D., Illian, J., Krainski, E., Simpson, D., and Lindgren, F. (2018). Spatial modeling with R-INLA: A review. *Wiley Interdisciplinary Reviews: Computational Statistics*, 10(6):e1443.
- Castro-Camilo, D., Mhalla, L., and Opitz, T. (2021). Bayesian space-time gap filling for inference on hot spots: an application to Red Sea surface temperatures. *Extremes*, 24:105–128.
- Coles, S. G. (1993). Regional modelling of extreme storms via max-stable processes. *Journal of the Royal Statistical Society: Series B (Methodological)*, 55(4):797–816.
- Cressie, N. A. C. (1993). *Statistics for spatial data (revised edition)*. Wiley, New York.
- Czado, C., Gneiting, T., and Held, L. (2009). Predictive model assessment for count data. *Biometrics*, 65(4):1254–1261.
- Davison, A. C. and Gholamrezaee, M. M. (2012). Geostatistics of extremes. *Proceedings of the Royal Statistical Society (Series A)*, 468(2138):581–608.

- de Fondeville, R. and Davison, A. C. (2018). High-dimensional peaks-over-threshold inference. *Biometrika*, 105(3):575–592.
- de Fondeville, R. and Davison, A. C. (2021). Functional peaks-over-threshold analysis. *arXiv preprint arXiv:2002.02711*.
- Dombry, C., Engelke, S., and Oesting, M. (2016). Exact simulation of max-stable processes. *Biometrika*, 103(2):303–317.
- Dombry, C. and Kabluchko, Z. (2018). Random tessellations associated with max-stable random fields. *Bernoulli*, 24(1):30–52.
- Dombry, C. and Ribatet, M. (2015). Functional regular variations, Pareto processes and peaks over threshold. *Statistics and Its Interface*, 8(1):9–17.
- Donlon, C. J., Martin, M., Stark, J., Roberts-Jones, J., Fiedler, E., and Wimmer, W. (2012). The operational sea surface temperature and sea ice analysis (OSTIA) system. *Remote Sensing of Environment*, 116:140–158.
- Drees, H. and Janßen, A. (2017). Conditional extreme value models: fallacies and pitfalls. *Extremes*, 20(4):777–805.
- Ferreira, A. and de Haan, L. (2014). The generalized Pareto process; with a view towards application and simulation. *Bernoulli*, 20(4):1717–1737.
- Fine, M., Cinar, M., Voolstra, C., Safa, A., Rinkevich, B., Laffoley, D., Hilmi, N., and Allemand, D. (2019). Coral reefs of the Red Sea - challenges and potential solutions. *Regional Studies in Marine Science*, 25:100498.
- Fuglstad, G.-A., Simpson, D., Lindgren, F., and Rue, H. (2019). Constructing priors that penalize the complexity of Gaussian random fields. *Journal of the American Statistical Association*, 114(525):445–452.
- Gneiting, T. and Raftery, A. E. (2007). Strictly proper scoring rules, prediction, and estimation. *Journal of the American statistical Association*, 102(477):359–378.
- Hazra, A. and Huser, R. (2021). Estimating high-resolution Red Sea surface temperature hotspots, using a low-rank semiparametric spatial model. *arXiv preprint arXiv:1912.05657*.
- Heffernan, J. E. and Resnick, S. I. (2007). Limit laws for random vectors with an extreme component. *The Annals of Applied Probability*, 17(2):537–571.
- Heffernan, J. E. and Stephenson, A. G. (2018). *ismev: An Introduction to Statistical Modeling of Extreme Values*. R package version 1.42.
- Heffernan, J. E. and Tawn, J. A. (2004). A conditional approach for multivariate extreme values (with discussion). *Journal of the Royal Statistical Society: Series B (Statistical Methodology)*, 66(3):497–546.
- Huser, R., Opitz, T., and Thibaud, E. (2017). Bridging asymptotic independence and dependence in spatial extremes using Gaussian scale mixtures. *Spatial Statistics*, 21(A):166–186.
- Huser, R., Opitz, T., and Thibaud, E. (2021). Max-infinitely divisible models and inference for spatial extremes. *Scandinavian Journal of Statistics*, 48(1):321–348.
- Huser, R. and Wadsworth, J. L. (2019). Modeling spatial processes with unknown extremal dependence class. *Journal of the American Statistical Association*, 114(525):434–444.

- Kabluchko, Z., Schlather, M., and de Haan, L. (2009). Stationary max-stable fields associated to negative definite functions. *Ann. Probab.*, 37(5):2042–2065.
- Keef, C., Tawn, J. A., and Lamb, R. (2013). Estimating the probability of widespread flood events. *Environmetrics*, 24(1):13–21.
- Kraïnski, E. T., Gómez-Rubio, V., Bakka, H., Lenzi, A., Castro-Camilo, D., Simpson, D., Lindgren, F., and Rue, H. (2018). *Advanced Spatial Modeling with Stochastic Partial Differential Equations Using R and INLA*. Chapman and Hall/CRC.
- Lindgren, F. and Rue, H. (2015). Bayesian spatial modelling with R-INLA. *Journal of Statistical Software*, 63(19):1–25.
- Lindgren, F., Rue, H., and Lindström, J. (2011). An explicit link between Gaussian fields and Gaussian Markov random fields: the stochastic partial differential equation approach. *Journal of the Royal Statistical Society: Series B (Statistical Methodology)*, 73(4):423–498.
- Opitz, T. (2017). Latent Gaussian modeling and INLA: A review with focus on space-time applications. *Journal of the French Statistical Society (Special Issue on Space-Time Statistics)*, 158(3):62–85.
- Opitz, T., Huser, R., Bakka, H., and Rue, H. (2018). INLA goes extreme: Bayesian tail regression for the estimation of high spatio-temporal quantiles. *Extremes*, 21(3):441–462.
- Padoan, S. A., Ribatet, M., and Sisson, S. A. (2010). Likelihood-based inference for max-stable processes. *Journal of the American Statistical Association*, 105(489):263–277.
- Richards, J. and Wadsworth, J. L. (2021). Spatial deformation for non-stationary extremal dependence. *Environmetrics*, 32:e2671.
- Rue, H. and Held, L. (2005). *Gaussian Markov Random Fields: Theory and Applications*. Chapman & Hall/CRC, Boca Raton.
- Rue, H., Martino, S., and Chopin, N. (2009). Approximate Bayesian inference for latent Gaussian models by using integrated nested Laplace approximations. *Journal of the Royal Statistical Society. Series B (Statistical Methodology)*, 71(2):319–392.
- Rue, H., Riebler, A., Sørbye, S. H., Illian, J. B., Simpson, D. P., and Lindgren, F. K. (2017). Bayesian computing with INLA: a review. *Annual Review of Statistics and Its Application*, 4:395–421.
- Schlather, M. (2002). Models for stationary max-stable random fields. *Extremes*, 5(1):33–44.
- Simpson, D., Rue, H., Riebler, A., Martins, T. G., and Sørbye, S. H. (2017). Penalising model component complexity: A principled, practical approach to constructing priors. *Statistical Science*, 32(1):1–28.
- Simpson, E. S. and Wadsworth, J. L. (2021). Conditional modelling of spatio-temporal extremes for Red Sea surface temperatures. *Spatial Statistics*, 41:100482.
- Smith, R. L. (1990). Max-stable processes and spatial extremes. Technical report.
- Smith, R. L. and Weissman, I. (1994). Estimating the extremal index. *Journal of the Royal Statistical Society. Series B (Methodological)*, 56(3):515–528.

- Soubeyrand, S. and Haon-Lasportes, E. (2015). Weak convergence of posteriors conditional on maximum pseudo-likelihood estimates and implications in ABC. *Statistics & Probability Letters*, 107:84–92.
- Strokorb, K., Ballani, F., and Schlather, M. (2015). Tail correlation functions of max-stable processes. *Extremes*, 18(2):241–271.
- Thibaud, E. and Opitz, T. (2015). Efficient inference and simulation for elliptical Pareto processes. *Biometrika*, 102(4):855–870.
- Tierney, L. and Kadane, J. B. (1986). Accurate approximations for posterior moments and marginal densities. *Journal of the American Statistical Association*, 81(393):82–86.
- van Niekerk, J., Bakka, H., Rue, H., and Schenk, L. (2019). New frontiers in Bayesian modeling using the INLA package in R. *arXiv preprint arXiv:1907.10426*.
- Vehtari, A., Gelman, A., and Gabry, J. (2017). Practical Bayesian model evaluation using leave-one-out cross-validation and WAIC. *Statistics and Computing*, 27(5):1413–1432.
- Wadsworth, J. L. and Tawn, J. A. (2019). Higher-dimensional spatial extremes via single site conditioning. *arXiv preprint arXiv:1912.06560*.
- Watanabe, S. (2013). A widely applicable Bayesian information criterion. *Journal of Machine Learning Research*, 14(1):867–897.
- Zhang, L., Shaby, B. A., and Wadsworth, J. L. (2021). Hierarchical transformed scale mixtures for flexible modeling of spatial extremes on datasets with many locations. *Journal of the American Statistical Association (to appear)*.

A Extremal dependence properties of the Red Sea data

In this section, we aim to assess some of the extremal dependence properties of the Red Sea data. To do this, we consider a non-limiting version of the tail correlation function $\chi(s, s+h)$ introduced in equation (1). In particular, we define

$$\chi_q(s, s+h) = \Pr \{F_L(X(s+h)) > q \mid F_L(X(s)) > q\},$$

for F_L denoting a standard Laplace distribution, $s, s+h \in \mathcal{S}$ with $X(s), X(s+h) \sim F_L$, and $q \in [0, 1]$. We are interested in values of q close to 1 in order to focus on extremal dependence properties. In Figure A, we provide empirical estimates of $\chi_q(s, s+h)$ for the Red Sea data, with $q = 0.9, 0.95, 0.99$, and s chosen to be the conditioning site s_0 used for inference in Sections 3.3 to 3.7. Estimates are shown for $s+h$ being each of the spatial locations in our dataset.

There are two reasons why we are interested in these plots. The first is to assess the type of extremal dependence exhibited by the data, so we can better understand the types of models that will be appropriate here. As the level q increases, it is clear that there is weakening dependence in the data. This suggests that models for asymptotic independence will be more appropriate than those for asymptotic dependence here, a finding that is reflected in the models we favour in both the spatial and spatio-temporal cases. The second use of these plots is to assess our assumption of isotropy. To do this, the spatial domain have been separated into eight sections, as shown in the top-left panel of Figure A, and we consider whether the extremal dependence behaviour differs within these sections. It appears that there is some violation of this assumption, since the results in the bottom-left quadrant are different to the others. Some ways to deal with this issue are discussed in Section 6.

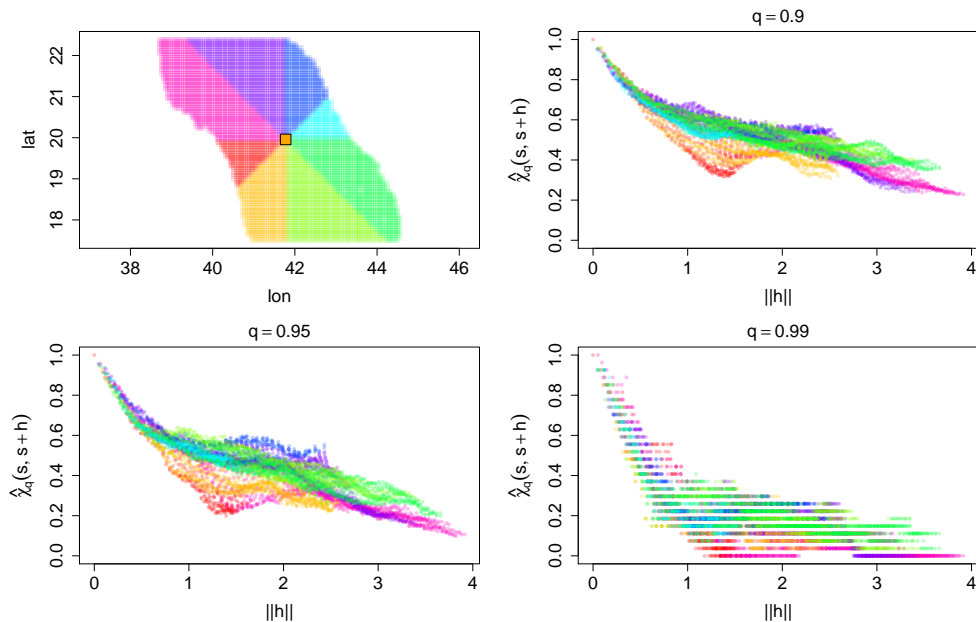


Figure 9: Estimates of $\chi_q(s, s+h)$ for all spatial locations, using one conditioning site (highlighted in orange), and for $q = 0.9, 0.95, 0.99$. The locations in the top-left panel have been divided into eight sections, with the $\chi_q(s, s+h)$ estimates in the remaining plots coloured accordingly.

B Additional model comparisons

B.1 A comparison of the two residual processes

In Section 5.4, we discussed the implementation of two different structures for the spatial residual process $\{Z^0(s)\}$, both of which ensure the constraint that $Z^0(s_0) = 0$ is fulfilled. Throughout the paper, we use a process of the form $\{Z(s)\} - Z(s_0)$, but the alternative is to use $\{Z(s)\} \mid Z(s_0) = 0$. In Table 4 we present WAIC results for the models described in Table 1 of Section 3.3 using both residual processes. Models 0 to 5 are applied to the moderate set of spatial locations shown in the right panel of Figure 2 (Model 6 is omitted as it involves no modeling of the residual process), with the threshold u taken as the 0.95 quantile of observations on the Laplace scale. The conditioning site lies towards the centre of the spatial domain, and the mesh and remaining tuning parameters are chosen as previously. Model 3 with the $\{Z(s)\} - Z(s_0)$ residual process, which is the one we focus on in Section 3.7, performs the best here. For any given model, the WAIC values are quite similar using the two residual processes, although the $\{Z(s)\} - Z(s_0)$ construction we have used throughout our analysis is favoured overall. This indicates that the choice of $\{Z^0(s)\}$ is not so critical here, and that we have made a reasonable choice in our modeling.

B.2 Sensitivity of model fits to SPDE parameter ζ

In Section 5.3, we gave an introduction to the SPDE approach, with parameter ν representing the shape parameter of the Matérn covariance. In the SPDE framework, this links to the parameter $\zeta = \nu + D/2$, i.e., in the spatial case $\zeta = \nu + 1$. The value of ζ must be fixed when implementing the INLA methodology, with $\zeta = 1.5$ corresponding to an exponential covariance, and $\zeta = 2$ providing smoother Gaussian realizations.

In Table 5, we compare WAIC values for each of the models in Table 1, for $\zeta = 1.5$ and $\zeta = 2$; all other modeling choices fixed as in Section 3. Model 4 with $\zeta = 1.5$ remains the most successful model, although selecting $\zeta = 1.5$ or $\zeta = 2$ is shown to have little effect for any of the models. We opt to fix $\zeta = 1.5$ throughout the paper, as we find

Model	$\{Z(s)\} - Z(s_0)$	$\{Z(s)\} \mid Z(s_0) = 0$
0	337	298
1	43	65
2	80	71
3	0	18
4	20	23
5	55	61

Table 4: Comparison of WAIC values for models fitted with different residual processes. The minimum WAIC value (-95298 for Model 3 with residual process $\{Z(s)\} - Z(s_0)$) has been subtracted from all other values. Results in bold demonstrate the minimum WAIC value achieved for each model.

this to perform slightly better overall, although the form of the model clearly has more of an effect on the results.

Model	$\zeta = 1.5$	$\zeta = 2$
0	2438	2447
1	614	624
2	743	746
3	4	15
4	0	12
5	611	639
6	4394961	4394960

Table 5: Comparison of WAIC values for models fitted with different values of ζ . The minimum WAIC value (-1460982 for Model 4 with $\zeta = 1.5$) has been subtracted from all other values. Results in bold demonstrate the minimum WAIC value achieved for each model.

C Histogram of PIT values for Model 3

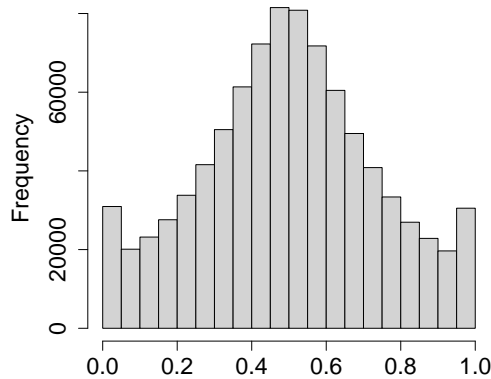


Figure 10: Histogram of PIT values for Model 3.

In Section 3.6, we discussed the use of the probability integral transform as a model fitting diagnostic. The idea is that the closer the PIT values are to being uniform in distribution, the better the model captures variability in

predictive distributions when predicting a single data point. In Figure 10, we present a histogram of these results for Model 3, with equivalent plots for the Models 0 to 5 being very similar to this one. We recall that since Model 6 does not allow for any residual variation, we are not suggesting it as a serious model contender, and do not consider an equivalent PIT histogram here.

Since we have smooth, gridded data and a flexible residual process, Models 0 to 5 provide almost perfect predictions. Plots such as this, relating to leave-one-out cross-validation, are therefore less relevant here than in other cases. The peak in the middle of the PIT histogram suggests that the posterior predictive densities $\pi(x_i | \mathbf{x}_{-i})$ are usually slightly too “flat” in many cases. It is useful to consider this information alongside the variance in posterior predictive distributions, which is much smaller for Model 3 than Model 6.